MULTISCALE MODEL. SIMUL.
Vol. 6, No. 1, pp. 319–346

A MULTISCALE MORTAR MIXED FINITE ELEMENT METHOD*

TODD ARBOGAST†, GERGINA PENCHEVA‡, MARY F. WHEELER§, AND IVAN YOTOV‡

Abstract. We develop multiscale mortar mixed finite element discretizations for second order elliptic equations. The continuity of flux is imposed via a mortar finite element space on a coarse grid scale, while the equations in the coarse elements (or subdomains) are discretized on a fine grid scale. The polynomial degree of the mortar and subdomain approximation spaces may differ; in fact, the mortar space achieves approximation comparable to the fine scale on its coarse grid by using higher order polynomials. Our formulation is related to, but more flexible than, existing multiscale finite element and variational multiscale methods. We derive a priori error estimates and show, with appropriate choice of the mortar space, optimal order convergence and some superconvergence on the fine scale for both the solution and its flux. We also derive efficient and reliable a posteriori error estimators, which are used in an adaptive mesh refinement algorithm to obtain appropriate subdomain and mortar grids. Numerical experiments are presented in confirmation of the theory.

Key words. multiscale, mixed finite element, mortar finite element, error estimates, a posteriori, superconvergence, multiblock, nonmatching grids

AMS subject classifications. 65N06, 65N12, 65N15, 65N22, 65N30

DOI. 10.1137/060662587

1. Introduction.

We consider a second order linear elliptic equation that, in porous medium applications, models single phase Darcy flow. We solve for the pressure p and the velocity $\mathbf{u}$ satisfying

$$\mathbf{u} = -K\nabla p \quad \text{in } \Omega, \tag{1.1}$$

$$\nabla \cdot \mathbf{u} = f \quad \text{in } \Omega, \tag{1.2}$$

$$p = g \quad \text{on } \partial\Omega, \tag{1.3}$$

where $\Omega \subset \mathbf{R}^d$, $d = 2$ or 3, is the domain and K is a symmetric, uniformly positive definite tensor with $L^\infty(\Omega)$-components representing the permeability divided by the viscosity. The Dirichlet boundary conditions are considered merely for simplicity. We suppose that the problem is at least $H^{3/2+\varepsilon}$-regular, for some $\varepsilon > 0$, where H^r is the standard Sobolev space of functions having rth order weak derivatives in L^2. We have H^2-regularity, for example, if $f \in L^2(\Omega)$, $g \in H^{3/2}(\Omega)$, the components of $K \in C^{0,1}(\bar{\Omega})$, and Ω is convex or $\partial\Omega$ is smooth enough (see [28, 34, 26]).

A number of papers deal with the analysis and implementation of mixed methods applied to the problem on conforming grids (see, e.g., [42, 39, 37, 15, 13, 14, 17, 21,

*Received by the editors June 9, 2006; accepted for publication (in revised form) January 3, 2007; published electronically May 7, 2007.

http://www.siam.org/journals/mms/6-1/66258.html

†Institute for Computational Engineering and Sciences and Department of Mathematics, The University of Texas at Austin, Austin, TX 78712 (arbogast@ices.utexas.edu). This author was supported by NSF grant DMS-0408489.

‡Department of Mathematics, 301 Thackeray Hall, University of Pittsburgh, Pittsburgh, PA 15260 (gepst12@math.pitt.edu, yotov@math.pitt.edu). These authors were supported by NSF grant DMS 0411694 and DOE grant DE-FG02-04ER25618.

§Institute for Computational Engineering and Sciences, Department of Aerospace Engineering and Engineering Mechanics, and Department of Petroleum and Geosystems Engineering, The University of Texas at Austin, Austin, TX 78712 (mfw@ices.utexas.edu). This author was supported by DOE grant DE-FGO2-04ER25617.

36, 43, 22, 24, 8, 6] and the books [40, 16]), on nested locally refined grids (see, e.g., [23, 25]), and on nonmatching grids [5, 9]. Another set of papers deals with multiscale approximation of the mixed system (see, e.g., [7, 18, 3, 1, 4, 2] and the related control volume work [33]).

It is difficult to solve (1.1)–(1.3) when Ω is large and the coefficient K is heterogeneous, varying on a fine scale. A straightforward approach to discretization would require full fine scale grid resolution of the variation in K over all of Ω, resulting in a large, highly coupled system of equations. Solution of this system would in many cases be computationally intractable.

To alleviate the computational burden, the variational multiscale method [31, 32, 12] and multiscale finite elements [29, 30] were developed for (1.1)–(1.3) written as a single second order partial differential equation. The mixed system of two first order equations was treated in a variational multiscale context in [7, 3, 1, 4, 2] and in a multiscale finite element method context in [18]. Up to relatively minor differences, these two approaches are equivalent [4].

In both methods, the problem (1.1)–(1.3) is decomposed into a series of small, local, coarse element (or subdomain) problems. These local problems are given appropriate boundary conditions and solved on the fine scale (to resolve variations in K) to define the coarse scale multiscale finite element basis. This coarse basis is then used to approximate the solution globally. Essentially, the problem is fully resolved on the fine scale, but the overall problem is solved using a reduced degree-of-freedom globally coupled system. The computational efficiency of the method comes from its divide-and-conquer strategy. The small, localized subproblems are much more effectively solved than the full system all at once. The coarse scale coupling involving only a few degrees of freedom per coarse element edge (or face) also results in a relatively small and easily solved system.

In this paper, we develop a new but similar multiscale approach based on domain decomposition theory [27] and mortar finite elements [11, 5]. The idea is simple: we divide Ω into a series of small subdomains (or coarse elements), over which we pose the original problem. We allow for geometrically nonconforming domain decompositions. We tie the subdomains together using a low degree-of-freedom mortar space defined on a coarse scale mortar grid. The mortar provides a natural Dirichlet pressure boundary condition for the subdomain problems, which can easily be solved because of their relatively small size. The (weak) velocity flux mismatch provides a criterion for updating the mortar pressure, and we iterate to convergence. By using a higher order mortar approximation, we are able to compensate for the coarseness of the grid scale and maintain good (fine scale) overall accuracy. This approach is more flexible than the variational multiscale method and multiscale finite elements, because it is easy to improve global accuracy by simply refining the local mortar grid where needed. That is, we can easily exploit adaptive meshing strategies to improve where necessary the strength of the global coupling.

We also present an error analysis of the method. Our analysis is *not* a classic multiscale analysis. However, we show that the solution can be well approximated by our technique, automatically using grid refinement and mortar approximation order enhancement, no matter the multiscale nature of the solution. That is, we detect the multiscale nature of the solution through a posteriori analysis of intermediate approximation results, rather than a priori through homogenization or some other technique.

The algebraic system resulting from the multiscale mortar method is solved in parallel using a nonoverlapping domain decomposition algorithm [46, 5] based on an

algorithm originally developed in [27]. The coupled system is reduced to a coarse mortar interface problem, which is solved via the conjugate gradient (CG) method. Each CG iteration requires the solution of fine scale subdomain problems. We employ an efficient balancing preconditioner [20, 38], which provides a very moderately growing condition number and number of iterations with refining the mortar grid or increasing the number of subdomains.

Our method is formulated in the next section. After defining some projection operators in section 3, we prove a priori error bounds in section 4. If h resolves the fine scale, and $H > h$ is the coarse mortar scale, and if m is the degree of the mortar approximating polynomials and $k = l$ is the order of the approximation for velocities and pressures, then we show that the velocity errors are $\mathcal{O}(H^{m+1/2} + h^{k+1})$ and the pressure errors are $\mathcal{O}(H^{m+3/2} + h^{k+1})$. Thus, if $m > k$, we can control the mortar error and prevent pollution of the solution. We also show several superconvergence estimates and estimates of the mortar pressure approximation itself.

In section 5, we turn our attention to a posteriori error estimation, so that we can control an adaptive mesh procedure for obtaining appropriate coarse mortar and fine subdomain grids. Finally, in section 6, we present the results of several numerical experiments that confirm and illustrate our theoretical results.

2. Formulation of the method. Let Ω be decomposed into nonoverlapping subdomain blocks Ω_i, so that $\overline{\Omega} = \cup_{i=1}^n \overline{\Omega}_i$ and $\Omega_i \cap \Omega_j = \emptyset$ for $i \neq j$. The blocks need not share complete faces; i.e., they need not form a conforming partition. Let $\Gamma_{i,j} = \partial\Omega_i \cap \partial\Omega_j$, $\Gamma = \cup_{1\le i<j\le n} \Gamma_{i,j}$, and $\Gamma_i = \partial\Omega_i \cap \Gamma = \partial\Omega_i \backslash \partial\Omega$ denote interior block interfaces. Let

$$\mathbf{V}_i = H(\mathrm{div};\Omega_i), \qquad \mathbf{V} = \bigoplus_{i=1}^n \mathbf{V}_i,$$

$$W_i = L^2(\Omega_i), \qquad W = \bigoplus_{i=1}^n W_i = L^2(\Omega),$$

$$M_{i,j} = H^{1/2}(\Gamma_{i,j}), \qquad M = \bigoplus_{1\le i<j\le n}^{n} M_{i,j}.$$

Following [5], a weak form of (1.1)–(1.3) asks for $\mathbf{u} \in \mathbf{V}$, $p \in W$, and $\lambda \in M$ such that, for each i,

$$(K^{-1}\mathbf{u}, \mathbf{v})_{\Omega_i} = (p, \nabla\cdot\mathbf{v})_{\Omega_i} - \langle \lambda, \mathbf{v}\cdot\nu_i\rangle_{\Gamma_i} - \langle g, \mathbf{v}\cdot\nu_i\rangle_{\partial\Omega_i\backslash\Gamma}, \quad \mathbf{v} \in \mathbf{V}_i, \tag{2.1}$$

$$(\nabla\cdot\mathbf{u}, w)_{\Omega_i} = (f, w)_{\Omega_i}, \qquad w \in W_i, \tag{2.2}$$

$$\sum_{i=1}^n \langle \mathbf{u}\cdot\nu_i, \mu\rangle_{\Gamma_i} = 0, \qquad \mu \in M, \tag{2.3}$$

where ν_i is the outer unit normal to $\partial\Omega_i$ (see also [16, pp. 91–92]). Note that λ is the pressure on the block interfaces Γ and that (2.3) enforces weak continuity of $\mathbf{u}\cdot\nu$ on each $\Gamma_{i,j}$.

2.1. The finite element approximation. Let $\mathcal{T}_{h,i}$ be a conforming, quasi-uniform affine finite element partition of Ω_i, $1 \le i \le n$, of maximal element diameter h_i. Note that we need quasi uniformity only on each subdomain (and only for the inverse inequality (3.18) below). Our method allows spatially varying h_i, but to simplify the analysis and concentrate on the mortar approximation, we let $h = \max_{1\le i\le n} h_i$

and analyze the method in terms of this single value h. Note also that we allow for the possibility that $\mathcal{T}_{h,i}$ and $\mathcal{T}_{h,j}$ need not align on $\Gamma_{i,j}$. Define $\mathcal{T}_h = \cup_{i=1}^n \mathcal{T}_{h,i}$, and let $\mathcal{E}_h$ be the union of all interior edges (or faces in three dimensions) not including the subdomain interfaces and the outer boundary. Let

$$\mathbf{V}_{h,i} \times W_{h,i} \subset \mathbf{V}_i \times W_i$$

be any of the usual mixed finite element spaces (e.g., those of [42, 39, 37, 15, 14, 13, 17]), and let $\mathbf{V}_h$ or, equivalently, $\mathbf{V}_h \cdot \nu$ contain the polynomials of degree k. Then let

$$\mathbf{V}_h = \bigoplus_{i=1}^n \mathbf{V}_{h,i}, \quad W_h = \bigoplus_{i=1}^n W_{h,i}.$$

Note that the normal components of vectors in $\mathbf{V}_h$ are continuous between elements within each block Ω_i but not across Γ.

Let the mortar interface mesh $\mathcal{T}_{H,i,j}$ be a quasi-uniform finite element partition of $\Gamma_{i,j}$ with maximal element diameter $H_{i,j}$. Let $H = \max_{1\le i,j\le n} H_{i,j}$. Define $\mathcal{T}^{\Gamma,H} = \cup_{1\le i<j\le n} \mathcal{T}_{H,i,j}$. For any $\tau \in \mathcal{T}_{H,i,j}$, let

$$E_\tau = \big\{E \in \mathcal{T}_h : \partial E \cap \tau \neq \emptyset\big\}.$$

Denote by $M_{H,i,j} \subset L^2(\Gamma_{i,j})$ the mortar space on $\Gamma_{i,j}$, containing either the continuous or discontinuous piecewise polynomials of degree m on $\mathcal{T}_{H,i,j}$, where m is at least $k+1$. We remark that $\mathcal{T}_{H,i,j}$ need not be conforming if $M_{H,i,j}$ is discontinuous, but our error analysis will require conformity. Now let

$$M_H = \bigoplus_{1\le i<j\le n} M_{H,i,j}$$

be the mortar finite element space on Γ. For each subdomain Ω_i, define a projection $\mathcal{Q}_{h,i} : L^2(\Gamma_i) \to \mathbf{V}_{h,i} \cdot \nu_i|_{\Gamma_i}$ such that, for any $\phi \in L^2(\Gamma_i)$,

$$\langle \phi - \mathcal{Q}_{h,i}\phi, \mathbf{v} \cdot \nu_i \rangle_{\Gamma_i} = 0, \quad \mathbf{v} \in \mathbf{V}_{h,i}. \tag{2.4}$$

We require that the following condition be satisfied [5], where in this paper $\|\cdot\|_{r,R}$ is the usual Sobolev norm of $H^r(R)$ (we may drop r if $r = 0$ and R if $R = \Omega$).

Assumption 2.1. Assume that there exists a constant C, independent of h and H, such that

$$\|\mu\|_{\Gamma_{i,j}} \le C(\|\mathcal{Q}_{h,i}\mu\|_{\Gamma_{i,j}} + \|\mathcal{Q}_{h,j}\mu\|_{\Gamma_{i,j}}), \quad \mu \in M_H, \quad 1 \le i < j \le n. \tag{2.5}$$

Condition (2.5) says that the mortar space cannot be too rich compared to the normal traces of the subdomain velocity spaces. Therefore, in what follows, we tacitly assume that $h \le H \le 1$. Condition (2.5) is not very restrictive, and it is easily satisfied in practice (see, e.g., [46, 38]). In the following, we treat any function $\mu \in M_H$ as extended by zero on $\partial\Omega$.

In the mixed finite element approximation of (2.1)–(2.2), we seek $\mathbf{u}_h \in \mathbf{V}_h$, $p_h \in W_h$, $\lambda_H \in M_H$ such that, for $1 \le i \le n$,

$$(K^{-1}\mathbf{u}_h, \mathbf{v})_{\Omega_i} = (p_h, \nabla \cdot \mathbf{v})_{\Omega_i} - \langle \lambda_H, \mathbf{v} \cdot \nu_i \rangle_{\Gamma_i} - \langle g, \mathbf{v} \cdot \nu_i \rangle_{\partial\Omega_i \setminus \Gamma}, \quad \mathbf{v} \in \mathbf{V}_{h,i}, \tag{2.6}$$

$$(\nabla \cdot \mathbf{u}_h, w)_{\Omega_i} = (f, w)_{\Omega_i}, \quad w \in W_{h,i}, \tag{2.7}$$

$$\sum_{i=1}^n \langle \mathbf{u}_h \cdot \nu_i, \mu \rangle_{\Gamma_i} = 0, \quad \mu \in M_H. \tag{2.8}$$

Strictly within each block Ω_i, we have a standard mixed finite element method, and (2.7) enforces local conservation over each grid cell. Moreover, $\mathbf{u}_h \cdot \nu$ is continuous on any element edge (or face) $e \not\subset \Gamma \cup \partial\Omega$, and (2.8) enforces weak continuity of flux across these interfaces with respect to the mortar space M_H.

The above method was defined in [5], except that H was comparable to h ($H = \mathcal{O}(h)$) and $m = k+1$ was one more than the degree of approximating polynomials in $\mathbf{V}_h$. In the present work, we weaken the discretization of Γ by taking larger elements of size H but compensating with a higher degree of approximation. The theoretical results of [5] no longer hold, since asymptotically we now take $H = \mathcal{O}(h^\alpha)$, with $\alpha < 1$.

2.2. A domain decomposition formulation. Define a bilinear form $d_H : L^2(\Gamma) \times L^2(\Gamma) \to \mathbf{R}$ by

$$d_H(\lambda, \mu) = \sum_{i=1}^{n} d_{H,i}(\lambda, \mu) = -\sum_{i=1}^{n} \langle \mathbf{u}_h^*(\lambda) \cdot \nu_i, \mu \rangle_{\Gamma_i},$$

where $(\mathbf{u}_h^*(\lambda), p_h^*(\lambda)) \in \mathbf{V}_h \times W_h$ solves

$$(K^{-1}\mathbf{u}_h^*(\lambda), \mathbf{v})_{\Omega_i} = (p_h^*(\lambda), \nabla \cdot \mathbf{v})_{\Omega_i} - \langle \lambda, \mathbf{v} \cdot \nu_i \rangle_{\Gamma_i}, \quad \mathbf{v} \in \mathbf{V}_{h,i}, \tag{2.9}$$

$$(\nabla \cdot \mathbf{u}_h^*(\lambda), w)_{\Omega_i} = 0, \quad w \in W_{h,i}, \tag{2.10}$$

for each $1 \le i \le n$. Also define a linear functional $g_H : L^2(\Gamma) \to \mathbf{R}$ by

$$g_H(\mu) = \sum_{i=1}^{n} g_{H,i}(\mu) = \sum_{i=1}^{n} \langle \bar{\mathbf{u}}_h \cdot \nu_i, \mu \rangle_{\Gamma_i},$$

where $(\bar{\mathbf{u}}_h, \bar{p}_h) \in \mathbf{V}_h \times W_h$ solves, for $1 \le i \le n$,

$$(K^{-1}\bar{\mathbf{u}}_h, \mathbf{v})_{\Omega_i} = (\bar{p}_h, \nabla \cdot \mathbf{v})_{\Omega_i} - \langle g, \mathbf{v} \cdot \nu_i \rangle_{\partial\Omega_i \setminus \Gamma}, \quad \mathbf{v} \in \mathbf{V}_{h,i}, \tag{2.11}$$

$$(\nabla \cdot \bar{\mathbf{u}}_h, w)_{\Omega_i} = (f, w)_{\Omega_i}, \quad w \in W_{h,i}. \tag{2.12}$$

It is straightforward to show (see [27, 5]) that the solution of

$$d_H(\lambda_H, \mu) = g_H(\mu), \quad \mu \in M_H, \tag{2.13}$$

generates the solution of (2.6)–(2.8) via

$$\mathbf{u}_h = \mathbf{u}_h^*(\lambda_H) + \bar{\mathbf{u}}_h, \quad p_h = p_h^*(\lambda_H) + \bar{p}_h. \tag{2.14}$$

The following is proved in [5].

LEMMA 2.1. *The interface bilinear form $d_H(\cdot,\cdot)$ is symmetric and positive semi-definite on $L^2(\Gamma)$. If (2.5) holds, then $d_H(\cdot,\cdot)$ is positive definite on M_H. Moreover,*

$$d_{H,i}(\mu, \mu) = (K^{-1}\mathbf{u}_h^*(\mu), \mathbf{u}_h^*(\mu))_{\Omega_i} \ge 0. \tag{2.15}$$

A substructuring domain decomposition algorithm based on an algorithm of Glowinski and Wheeler [27] can be used to solve the linear system of equations resulting from (2.6)–(2.8) very efficiently in parallel. It solves the mortar interface problem (2.13) using the CG method with balancing preconditioner. See [5, 38] for more details.

3. Some projection operators and the weakly continuous velocities. We first introduce some projection operators needed in the analysis. Let $\mathcal{I}_H^c$ be the nodal interpolant operator into the space M_H^c, which is the subset of continuous functions in M_H (where we must use the Scott–Zhang operator [41] to define the nodal values of ψ if ψ is not smooth enough to form $\mathcal{I}_H^c\psi$ directly). For any $\varphi \in L^2(\Omega)$, let $\hat{\varphi} \in W_h$ be its $L^2(\Omega)$-projection satisfying

$$(\varphi - \hat{\varphi}, w) = 0, \quad w \in W_h.$$

Similarly, let $\mathcal{P}_H$ denote the $L^2(\Gamma)$-projection onto M_H. We already have (2.4), which defines the projection $\mathcal{Q}_{h,i} : L^2(\Gamma_i) \to \mathbf{V}_{h,i} \cdot \nu_i|_{\Gamma_i}$.

We recall that, for any of the standard mixed spaces,

$$\nabla \cdot \mathbf{V}_{h,i} = W_{h,i},$$

and there exists a projection Π_i of $(H^\varepsilon(\Omega_i))^d \cap \mathbf{V}_i$ onto $\mathbf{V}_{h,i}$ (for any $\varepsilon > 0$) satisfying that, for any $\mathbf{q} \in (H^\varepsilon(\Omega_i))^d \cap \mathbf{V}_i$,

$$\nabla \cdot \Pi_i \mathbf{q} = \widehat{\nabla \cdot \mathbf{q}}, \tag{3.1}$$

$$(\Pi_i \mathbf{q}) \cdot \nu_i = \mathcal{Q}_{h,i}(\mathbf{q} \cdot \nu_i). \tag{3.2}$$

Moreover (see [35, 5]),

$$\|\Pi_i \mathbf{q}\|_{\Omega_i} \le C(\|\mathbf{q}\|_{\varepsilon,\Omega_i} + \|\nabla \cdot \mathbf{q}\|_{\Omega_i}). \tag{3.3}$$

We assume that the order of approximation of $W_{h,i}$ is $l+1$ (and recall that $\mathbf{V}_{h,i}$ is $k+1$ and M_H is $m+1$). In all cases, $l = k$ or $l = k-1$, and we have assumed for simplicity that the order of approximation is the same on every subdomain. Our projection operators have the following approximation properties:

$$\|\psi - \mathcal{I}_H^c\psi\|_{t,\Gamma_{i,j}} \le C\|\psi\|_{s,\Gamma_{i,j}} H^{s-t}, \qquad 0 \le s \le m+1, \quad 0 \le t \le 1, \tag{3.4}$$

$$\|\psi - \mathcal{P}_H\psi\|_{-t,\Gamma_{i,j}} \le C\|\psi\|_{s,\Gamma_{i,j}} H^{s+t}, \qquad 0 \le s \le m+1, \quad 0 \le t \le 1, \tag{3.5}$$

$$\|\varphi - \hat{\varphi}\| \le C\|\varphi\|_t h^t, \qquad 0 \le t \le l+1, \tag{3.6}$$

$$\|\nabla \cdot (\mathbf{q} - \Pi_i \mathbf{q})\|_{\Omega_i} \le C\|\nabla \cdot \mathbf{q}\|_{t,\Omega_i} h^t, \qquad 0 \le t \le l+1, \tag{3.7}$$

$$\|\mathbf{q} - \Pi_i \mathbf{q}\|_{\Omega_i} \le C\|\mathbf{q}\|_{r,\Omega_i} h^r, \qquad 1 \le r \le k+1, \tag{3.8}$$

$$\|\psi - \mathcal{Q}_{h,i}\psi\|_{-t,\Gamma_{i,j}} \le C\|\psi\|_{r,\Gamma_{i,j}} h^{r+t}, \qquad 0 \le r \le k+1, \quad 0 \le t \le k+1, \tag{3.9}$$

$$\|(\mathbf{q} - \Pi_i \mathbf{q}) \cdot \nu_i\|_{-t,\Gamma_{i,j}} \le C\|\mathbf{q}\|_{r,\Gamma_{i,j}} h^{r+t}, \quad 0 \le r \le k+1, \quad 0 \le t \le k+1, \tag{3.10}$$

where $\|\cdot\|_{-t}$ is the norm of H^{-t}, the dual of H^t (*not* H_0^t). Bounds (3.5)–(3.7) and (3.9)–(3.10) are standard L^2-projection approximation results [19]; bound (3.8) can be found in [16, 40]; and (3.4) is a standard interpolation bound [19].

For theoretical purposes, it is convenient to define the space of weakly continuous velocities, which is the space

$$\mathbf{V}_{h,0} = \left\{ \mathbf{v} \in \mathbf{V}_h : \sum_{i=1}^n \langle \mathbf{v}|_{\Omega_i} \cdot \nu_i, \mu \rangle_{\Gamma_i} = 0 \quad \forall\, \mu \in M_H \right\}.$$

We note that we can eliminate λ_H from the mixed method (2.6)–(2.8) by restricting $\mathbf{V}_h$ to $\mathbf{V}_{h,0}$; that is, the problem is equivalent to finding $\mathbf{u}_h \in \mathbf{V}_{h,0}$ and $p_h \in W_h$ such that

$$(K^{-1}\mathbf{u}_h, \mathbf{v}) = \sum_{i=1}^{n} (p_h, \nabla \cdot \mathbf{v})_{\Omega_i} - \langle g, \mathbf{v} \cdot \nu \rangle_{\partial\Omega}, \quad \mathbf{v} \in \mathbf{V}_{h,0}, \tag{3.11}$$

$$\sum_{i=1}^{n} (\nabla \cdot \mathbf{u}_h, w)_{\Omega_i} = (f, w), \qquad w \in W_h. \tag{3.12}$$

LEMMA 3.1. *Under hypothesis* (2.5)*, there exists a projection operator* $\Pi_0 : (H^{1/2+\varepsilon}(\Omega)) \cap \mathbf{V} \to \mathbf{V}_{h,0}$ *such that*

$$(\nabla \cdot (\Pi_0 \mathbf{q} - \mathbf{q}), w)_\Omega = 0, \quad w \in W_h, \tag{3.13}$$

and

$$\|\Pi_0 \mathbf{q} - \Pi \mathbf{q}\| \le C \sum_{i=1}^{n} \|\mathbf{q}\|_{r+1/2,\Omega_i} h^r H^{1/2}, \qquad 0 \le r \le k+1, \tag{3.14}$$

$$\|\Pi_0 \mathbf{q} - \mathbf{q}\| \le C \sum_{i=1}^{n} \big(\|\mathbf{q}\|_{r,\Omega_i} h^r + \|\mathbf{q}\|_{r+1/2,\Omega_i} h^r H^{1/2} \big), \quad 1 \le r \le k+1, \tag{3.15}$$

$$\|\Pi_0 \mathbf{q} - \mathbf{q}\| \le C \sum_{i=1}^{n} \|\mathbf{q}\|_{r,\Omega_i} h^{r-1/2} H^{1/2}, \qquad 1 \le r \le k+1, \tag{3.16}$$

wherein $\Pi \mathbf{q}|_{\Omega_i} = \Pi_i \mathbf{q}$.

The proof of this lemma can be found in [5, sect. 3], with a straightforward modification of the argument for the two scales h and H. It is now easy to prove solvability of our method.

LEMMA 3.2. *If* (2.5) *holds, then there exists a unique solution of* (2.6)–(2.8).

Proof. Uniqueness for vanishing data implies general existence and uniqueness for finite-dimensional square linear systems, and so assume f and g vanish. Take $\mathbf{v} = \mathbf{u}_h \in \mathbf{V}_{h,0}$ in (3.11)–(3.12) to conclude that $\mathbf{u}_h = 0$. Given $p_h \in W_h$, there is a vector field $\mathbf{q}$ such that $\nabla \cdot \mathbf{q} = p_h$, and so take $\mathbf{v} = \Pi_0 \mathbf{q}$ to conclude that $0 = \sum_i (p_h, \nabla \cdot \Pi_0 \mathbf{q})_{\Omega_i} = (p_h, \nabla \cdot \mathbf{q})_\Omega = \|p_h\|^2$, implying that $p_h = 0$. Now, returning to (2.6), we have that $0 = \langle \lambda_H, \mathbf{v} \cdot \nu_i \rangle_{\Gamma_i} = \langle \mathcal{Q}_{h,i} \lambda_H, \mathbf{v} \cdot \nu_i \rangle_{\Gamma_i}$ for any $\mathbf{v} \in \mathbf{V}_{h,i}$. Again, we can find some $\mathbf{v}$ so that $\mathbf{v} \cdot \nu_i = \mathcal{Q}_{h,i} \lambda_H$, which implies that $\mathcal{Q}_{h,i} \lambda_H = 0$. Finally, (2.5) shows that $\lambda_H = 0$, and the proof is complete. ∎

In the analysis, we will use the nonstandard trace theorem

$$\|q\|_{r,\Gamma_{i,j}} \le C \|q\|_{r+1/2,\Omega_i}, \quad 0 < r \tag{3.17}$$

(see [28, Thm. 1.5.2.1]), the local inverse inequality

$$\|\mathbf{v} \cdot \nu\|_{\partial\Omega_i} \le C h^{-1/2} \|\mathbf{v}\|_{\Omega_i} \tag{3.18}$$

for any function $\mathbf{v} \in \mathbf{V}_{h,i}$ (see [5, Lem. 4.1]), and the bound (see [39, 16])

$$\langle q, \mathbf{v} \cdot \nu \rangle_{\partial\Omega_i} \le C \|q\|_{1/2,\partial\Omega_i} \|\mathbf{v}\|_{H(\mathrm{div};\Omega_i)}. \tag{3.19}$$

4. A priori error estimates. Subtracting (3.11)–(3.12) from (2.1)–(2.2) gives the following equations for the error (recall that $\lambda = p$):

$$(K^{-1}(\mathbf{u} - \mathbf{u}_h), \mathbf{v}) = \sum_{i=1}^{n} \big((p - p_h, \nabla \cdot \mathbf{v})_{\Omega_i} - \langle p, \mathbf{v} \cdot \nu_i \rangle_{\Gamma_i} \big), \quad \mathbf{v} \in \mathbf{V}_{h,0}, \tag{4.1}$$

$$\sum_{i=1}^{n} (\nabla \cdot (\mathbf{u} - \mathbf{u}_h), w)_{\Omega_i} = 0, \qquad w \in W_h. \tag{4.2}$$

4.1. A priori estimates for the velocity.

THEOREM 4.1. *For the velocity* $\mathbf{u}_h$ *of the mixed method* (2.6)–(2.8)*, if* (2.5) *holds, then there exists a positive constant* C*, independent of* h *and* H*, such that*

(4.3)
$$\|\nabla\cdot(\mathbf{u}-\mathbf{u}_h)\| \le C\sum_{i=1}^{n}\|\nabla\cdot\mathbf{u}\|_{r,\Omega_i}h^r, \quad 0\le r\le l+1,$$

(4.4)
$$\|\mathbf{u}-\mathbf{u}_h\| \le C\sum_{i=1}^{n}\big(\|p\|_{s+1/2,\Omega_i}H^{s-1/2} + \|\mathbf{u}\|_{r,\Omega_i}h^r + \|\mathbf{u}\|_{r+1/2,\Omega_i}h^rH^{1/2}\big), \quad 1\le r\le k+1, \quad 0<s\le m+1.$$

Remark 4.1. A straightforward modification of the argument in [5, sect. 4] produces error estimates for $\|\mathbf{u}-\mathbf{u}_h\|$ of order $\mathcal{O}(H^sh^{-1/2}+h^r)$, which at its limits is $\mathcal{O}(H^{m+1}h^{-1/2}+h^{k+1})$. This is asymptotically undesirable as $h\to 0$. In our improved estimate, we obtain a balancing of the terms in (4.4) when $H=\mathcal{O}(h^{r/(s-1/2)})$, which at its limits is $H=\mathcal{O}(h^{(k+1)/(m+1/2)})$. For the lowest order Raviart–Thomas–Nédélec (RTN) space RTN_0 [39, 37], $k=l=0$, and so if, say, $m=2$, then we should take the asymptotic scaling $H=\mathcal{O}(h^{2/5})$, which maintains the optimal convergence rate $\mathcal{O}(h)$.

Proof. The divergence error is trivial to estimate from (4.2) using $w=\nabla\cdot(\Pi\mathbf{u}-\mathbf{u}_h)\in W_h$ and (3.7). Note also that $\nabla\cdot\Pi_0\mathbf{u}=\nabla\cdot\mathbf{u}_h=\hat{f}=\widehat{\nabla\cdot\mathbf{u}}$.

We take $\mathbf{v}=\Pi_0\mathbf{u}-\mathbf{u}_h\in\mathbf{V}_{h,0}$ and $w=\hat{p}-p_h$ in (4.1)–(4.2), sum the equations, and note that $\sum_i\langle\mathcal{I}_H^cp,\mathbf{v}\cdot\nu_i\rangle_{\Gamma_i}=0$ for any $\mathbf{v}\in\mathbf{V}_{h,0}$ to get

(4.5)
$$\begin{aligned}
&(K^{-1}(\Pi_0\mathbf{u}-\mathbf{u}_h),\Pi_0\mathbf{u}-\mathbf{u}_h)\\
&\quad=\sum_{i=1}^{n}\langle\mathcal{I}_H^cp-p,(\Pi_0\mathbf{u}-\mathbf{u}_h)\cdot\nu_i\rangle_{\Gamma_i}+(K^{-1}(\Pi_0\mathbf{u}-\mathbf{u}),\Pi_0\mathbf{u}-\mathbf{u}_h)\\
&\quad\le\sum_{i=1}^{n}\|\mathcal{I}_H^cp-p\|_{1/2,\partial\Omega_i}\|\Pi_0\mathbf{u}-\mathbf{u}_h\|_{H(\mathrm{div};\Omega_i)}+(K^{-1}(\Pi_0\mathbf{u}-\mathbf{u}),\Pi_0\mathbf{u}-\mathbf{u}_h)\\
&\quad\le C\bigg(\sum_{i=1}^{n}\|p\|_{s+1/2,\Omega_i}H^{s-1/2}\|\Pi_0\mathbf{u}-\mathbf{u}_h\|_{\Omega_i}\\
&\qquad+\sum_{i=1}^{n}\big(\|\mathbf{u}\|_{r,\Omega_i}h^r+\|\mathbf{u}\|_{r+1/2,\Omega_i}h^rH^{1/2}\big)\|\Pi_0\mathbf{u}-\mathbf{u}_h\|\bigg),
\end{aligned}$$

for $1\le r\le k+1$, $0<s\le m+1$, where we used (3.4), (3.17), and (3.15), and that $\nabla\cdot(\Pi_0\mathbf{u}-\mathbf{u}_h)=0$. An application of the Cauchy–Schwarz inequality completes the proof. ∎

If we restrict to the case of diagonal tensor K and RTN spaces [39, 37] on rectangular grids, we can obtain superconvergence of the velocity at certain discrete points. For a function ψ and a (say, three-dimensional) rectangular element E, let $|||\psi|||_{i,E}^2$ denote the approximate integral of $|\psi|^2$ using exact integration in x_i and the $k+1$ point Gauss rule in the other directions. Then let

(4.6)
$$|||\mathbf{q}|||^2=\sum_{i=1}^{3}\sum_{E\in\mathcal{T}_h}|||q_i|||_{i,E}^2,$$

and note that if $\mathbf{v} \in \mathbf{V}_h$, then $|||\mathbf{v}||| = \|\mathbf{v}\|_\Omega$.

THEOREM 4.2. *Assume that the tensor K is diagonal and the mixed finite element spaces are RTN on rectangular grids. For the velocity $\mathbf{u}_h$ of the mixed method (2.6)–(2.8), if (2.5) holds, then there exists a positive constant C, independent of h and H, such that*

$$|||\mathbf{u} - \mathbf{u}_h||| \le C \sum_{i=1}^{n} \big(\|p\|_{s+1/2,\Omega_i} H^{s-1/2} + \|\mathbf{u}\|_{r+1/2,\Omega_i} h^r H^{1/2} \big), \tag{4.7}$$

where $1/2 \le r \le k+1$, $0 < s \le m+1$.

Proof. We need two well-known results about superconvergence on the subdomains. First, Π is superclose to the weighted L^2-projection (see [36] and [22, Thm. 3.1]), which translates into

$$(K^{-1}(\Pi\mathbf{u} - \mathbf{u}), \Pi_0\mathbf{u} - \mathbf{u}_h)_{\Omega_i} \le C\|\mathbf{u}\|_{r+1,\Omega_i} h^{r+1} \|\Pi_0\mathbf{u} - \mathbf{u}_h\|_{\Omega_i}, \quad 0 \le r \le k+1.$$

Second, the usual mixed method Π operator exhibits superconvergence (see [22]):

$$|||\mathbf{u} - \Pi\mathbf{u}|||_{\Omega_i} \le C\|\mathbf{u}\|_{r+1,\Omega_i} h^{r+1}, \quad 0 \le r \le k+1. \tag{4.8}$$

To use the former estimate, we revisit part of (4.5) and estimate the term

$$\begin{aligned}
&(K^{-1}(\Pi_0\mathbf{u} - \mathbf{u}), \Pi_0\mathbf{u} - \mathbf{u}_h)_{\Omega_i} \\
&\quad = (K^{-1}(\Pi_0\mathbf{u} - \Pi\mathbf{u}), \Pi_0\mathbf{u} - \mathbf{u}_h)_{\Omega_i} + (K^{-1}(\Pi\mathbf{u} - \mathbf{u}), \Pi_0\mathbf{u} - \mathbf{u}_h)_{\Omega_i} \\
&\quad \le C\big(\|\Pi_0\mathbf{u} - \Pi\mathbf{u}\|_{\Omega_i} + \|\mathbf{u}\|_{r+1/2,\Omega_i} h^{r+1/2} \big) \|\Pi_0\mathbf{u} - \mathbf{u}_h\|_{\Omega_i}
\end{aligned}$$

for $1/2 \le r \le k + 3/2$. Thus with (3.14), the bound in (4.5) is improved to

$$\|\Pi_0\mathbf{u} - \mathbf{u}_h\| \le C \sum_{i=1}^{n} \big(\|p\|_{s+1/2,\Omega_i} H^{s-1/2} + \|\mathbf{u}\|_{r+1/2,\Omega_i} h^r H^{1/2} \big), \tag{4.9}$$

where $1/2 \le r \le k+1$ and $0 < s \le m+1$. Finally,

$$\begin{aligned}
|||\mathbf{u} - \mathbf{u}_h||| &\le |||\mathbf{u} - \Pi\mathbf{u}||| + |||\Pi\mathbf{u} - \Pi_0\mathbf{u}||| + |||\Pi_0\mathbf{u} - \mathbf{u}_h||| \\
&= |||\mathbf{u} - \Pi\mathbf{u}||| + \|\Pi\mathbf{u} - \Pi_0\mathbf{u}\| + \|\Pi_0\mathbf{u} - \mathbf{u}_h\|,
\end{aligned}$$

and so a combination of the above estimates and (3.14) completes the proof. ∎

Remark 4.2. For RTN_0 ($k = l = 0$), the terms in (4.7) are balanced if $H = \mathcal{O}(h^{1/m})$, giving the superconvergence error $\mathcal{O}(h^{1+1/2m})$. For $m = 2$, this is $H = \mathcal{O}(h^{1/2})$, which differs slightly from the optimal choice $\mathcal{O}(h^{2/5})$ from Remark 4.1.

4.2. A priori estimates for the pressure.

THEOREM 4.3. *Assume full H^2-regularity of the problem on Ω. For the pressure p_h of the mixed method (2.6)–(2.8), if (2.5) holds, then there exists a positive constant C, independent of h and H, such that*

$$\begin{aligned}
\|\hat{p} - p_h\| \le C \sum_{i=1}^{n} \big(&\|p\|_{s+1/2,\Omega_i} H^{s+1/2} + \|\nabla\cdot\mathbf{u}\|_{t,\Omega_i} h^t H \\
&+ \|\mathbf{u}\|_{r,\Omega_i} h^r H + \|\mathbf{u}\|_{r+1/2,\Omega_i} h^r H^{3/2} \big),
\end{aligned} \tag{4.10}$$

$$\|p - p_h\| \le C \sum_{i=1}^{n} \|p\|_{t,\Omega_i} h^t + \|\hat{p} - p_h\|, \tag{4.11}$$

where $1 \le r \le k+1$, $0 < s \le m+1$, and $0 \le t \le l+1$.

Remark 4.3. Again, a straightforward modification of the argument in [5] produces an undesirable superconvergence error estimate of order $\mathcal{O}\big(H^{m+2}h^{-1/2} + H^{3/2}h^{k+1/2} + h^{l+2}\big)$ instead of $\mathcal{O}\big(H^{m+3/2} + H(h^{l+1} + h^{k+1})\big)$. A balancing of the terms in (4.10) implies for spaces with $l = k$ that $H = \mathcal{O}(h^{(k+1)/(m+1/2)})$, which gives superconvergence of order $\mathcal{O}(h^{(k+1)(m+3/2)/(m+1/2)})$. For $k = 0$ and $m = 2$, we should take the asymptotic scaling $H = \mathcal{O}(h^{2/5})$, which gives $\mathcal{O}(h^{7/5})$. If $H = \mathcal{O}(h^{1/m})$, as in Remark 4.2, then we expect an error of $\mathcal{O}(h^{1+1/m})$ when $k = l = 0$.

Proof. The proof uses a duality argument. Let φ be the solution of

$$\begin{aligned} -\nabla \cdot K\nabla\varphi &= -(\hat{p} - p_h) \quad \text{in } \Omega, \\ \varphi &= 0 \qquad\qquad\quad \text{on } \partial\Omega, \end{aligned}$$

and note that by elliptic regularity,

$$\|\varphi\|_2 \le C\|\hat{p} - p_h\|. \tag{4.12}$$

Take $\mathbf{v} = \Pi_0 K\nabla\varphi$ in (4.1) and use the weak continuity of $\mathbf{v}$ to see that

$$\begin{aligned} \|\hat{p} - p_h\|^2 &= \sum_{i=1}^n (\hat{p} - p_h, \nabla \cdot \Pi_0 K\nabla\varphi)_{\Omega_i} \\ &= \sum_{i=1}^n \big[(K^{-1}(\mathbf{u} - \mathbf{u}_h), \Pi_0 K\nabla\varphi)_{\Omega_i} + \langle p - \mathcal{P}_H p, \Pi_0 K\nabla\varphi \cdot \nu_i\rangle_{\Gamma_i}\big]. \end{aligned} \tag{4.13}$$

The first term on the right-hand side is easily estimated as

$$\begin{aligned} &\sum_{i=1}^n (K^{-1}(\mathbf{u} - \mathbf{u}_h), \Pi_0 K\nabla\varphi)_{\Omega_i} \\ &\quad = \sum_{i=1}^n \big[(K^{-1}(\mathbf{u} - \mathbf{u}_h), \Pi_0 K\nabla\varphi - K\nabla\varphi)_{\Omega_i} + (\mathbf{u} - \mathbf{u}_h, \nabla\varphi)_{\Omega_i}\big] \\ &\quad = \sum_{i=1}^n \big[(K^{-1}(\mathbf{u} - \mathbf{u}_h), \Pi_0 K\nabla\varphi - K\nabla\varphi)_{\Omega_i} \\ &\qquad\qquad - (\nabla \cdot (\mathbf{u} - \mathbf{u}_h), \varphi - \hat{\varphi})_{\Omega_i} + \langle (\mathbf{u} - \mathbf{u}_h) \cdot \nu_i, \varphi - \mathcal{P}_H\varphi\rangle_{\Gamma_i}\big] \\ &\quad \le C \sum_{i=1}^n \big(\|\mathbf{u} - \mathbf{u}_h\|_{\Omega_i}\sqrt{hH} + \|\nabla \cdot (\mathbf{u} - \mathbf{u}_h)\|_{\Omega_i} h \\ &\qquad\qquad + \|\mathbf{u} - \mathbf{u}_h\|_{H(\mathrm{div};\Omega_i)} H\big)\|\varphi\|_{2,\Omega_i}, \end{aligned} \tag{4.14}$$

using (3.16), (3.6), and (3.4), where $C = C(\max_i \|K\|_{1,\infty,\Omega_i})$. For the second term on the right-hand side in (4.13), we have

$$\begin{aligned} &\langle p - \mathcal{P}_H p, \Pi_0 K\nabla\varphi \cdot \nu_i\rangle_{\Gamma_i} \\ &\quad = \langle p - \mathcal{P}_H p, (\Pi_0 K\nabla\varphi - \Pi_i K\nabla\varphi) \cdot \nu_i + (\Pi_i K\nabla\varphi - K\nabla\varphi) \cdot \nu_i + K\nabla\varphi \cdot \nu_i\rangle_{\Gamma_i} \\ &\quad \le \sum_j \|p - \mathcal{P}_H p\|_{\Gamma_{i,j}} \big(\|(\Pi_0 K\nabla\varphi - \Pi_i K\nabla\varphi) \cdot \nu_i\|_{\Gamma_{i,j}} \\ &\qquad\qquad + \|(\Pi_i K\nabla\varphi - K\nabla\varphi) \cdot \nu_i\|_{\Gamma_{i,j}}\big) \\ &\qquad + \sum_j \|p - \mathcal{P}_H p\|_{-1/2,\Gamma_{i,j}} \|K\nabla\varphi \cdot \nu_i\|_{1/2,\Gamma_{i,j}} \\ &\quad \le CH^{s+1/2}\|p\|_{s+1/2,\Omega_i}\|\varphi\|_{2,\Omega_i}, \quad 0 < s \le m+1, \end{aligned} \tag{4.15}$$

using (3.5), (3.18), (3.14), and (3.10). The proof of (4.10) is completed by Theorem 4.1 and (3.8). Finally, (4.11) follows from (4.10) and (3.6). ∎

4.3. A priori estimates for the mortar pressure. Let $\|\cdot\|_{d_H}$ be the seminorm induced by $d_H(\cdot,\cdot)$ on $L^2(\Gamma)$, which is

$$\|\mu\|_{d_H} = d_H(\mu,\mu)^{1/2}, \quad \mu \in L^2(\Gamma).$$

THEOREM 4.4. *For the mortar pressure λ_H of the mixed method* (2.6)–(2.8)*, if* (2.5) *holds, then there exists a positive constant C, independent of h and H, such that*

$$\|p-\lambda_H\|_{d_H} \le C\Big\{\sum_{i=1}^{n}\big(\|p\|_{r+1,\Omega_i}+\|\mathbf{u}\|_{r,\Omega_i}\big)h^r + \|\mathbf{u}-\mathbf{u}_h\|\Big\}, \quad 1\le r\le k+1. \tag{4.16}$$

In the case of diagonal tensor K and RTN spaces on rectangular type grids,

$$\|p-\lambda_H\|_{d_H} \le C\Big\{\sum_{i=1}^{n}\|\mathbf{u}\|_{r+1,\Omega_i}h^{r+1} + |||\mathbf{u}-\mathbf{u}_h|||\Big\}, \quad 0\le r\le k+1. \tag{4.17}$$

Proof. For $\mu\in L^2(\Gamma)$, let

$$\mathbf{u}_h(\mu) = \mathbf{u}_h^*(\mu)+\bar{\mathbf{u}}_h, \quad p_h(\mu) = p_h^*(\mu)+\bar{p}_h,$$

and note that $(\mathbf{u}_h(\mu),p_h(\mu))\in \mathbf{V}_h\times W_h$ satisfies

$$\begin{aligned}(K^{-1}\mathbf{u}_h(\mu),\mathbf{v})_{\Omega_i} &= (p_h(\mu),\nabla\cdot\mathbf{v})_{\Omega_i} - \langle\mu,\mathbf{v}\cdot\nu\rangle_{\Gamma_i}\\ &\quad - \langle g,\mathbf{v}\cdot\nu\rangle_{\partial\Omega_i\setminus\Gamma}, && \mathbf{v}\in\mathbf{V}_{h,i},\end{aligned} \tag{4.18}$$

$$(\nabla\cdot\mathbf{u}_h(\mu),w)_{\Omega_i} = (f,w)_{\Omega_i}, \qquad w\in W_{h,i}. \tag{4.19}$$

In particular, $\mathbf{u}_h(\lambda_H)=\mathbf{u}_h$ and $p_h(\lambda_H)=p_h$. Since $\mathbf{u}_h^*(\cdot)$ is linear, (2.15) implies that

$$\begin{aligned}\|p-\lambda_H\|_{d_H} &\le C\|\mathbf{u}_h^*(p)-\mathbf{u}_h^*(\lambda_H)\| = C\|\mathbf{u}_h(p)-\mathbf{u}_h(\lambda_H)\|\\ &= C\|\mathbf{u}_h(p)-\mathbf{u}_h\| \le C\big(\|\mathbf{u}_h(p)-\mathbf{u}\|+\|\mathbf{u}-\mathbf{u}_h\|\big).\end{aligned} \tag{4.20}$$

Bound (4.16) now follows from Theorem 4.1 and the standard mixed method estimate for (2.1)–(2.2) and (4.18)–(4.19) [42, 39, 21]:

$$\|\mathbf{u}_h(p)-\mathbf{u}\|_{\Omega_i} \le C(\|p\|_{r+1,\Omega_i}+\|\mathbf{u}\|_{r,\Omega_i})h^r, \quad 1\le r\le k+1.$$

To show (4.17), we modify (4.20) as

$$\begin{aligned}\|\mathbf{u}_h(p)-\mathbf{u}_h\| &\le \|\mathbf{u}_h(p)-\Pi\mathbf{u}\|+\|\Pi\mathbf{u}-\mathbf{u}_h\|\\ &= \|\mathbf{u}_h(p)-\Pi\mathbf{u}\|+|||\Pi\mathbf{u}-\mathbf{u}_h|||\\ &\le \|\mathbf{u}_h(p)-\Pi\mathbf{u}\|+|||\Pi\mathbf{u}-\mathbf{u}|||+|||\mathbf{u}-\mathbf{u}_h|||,\end{aligned} \tag{4.21}$$

and we apply the superconvergence estimate for Π (4.8) and a superconvergence estimate for the standard mixed method

$$\|\mathbf{u}_h(p)-\Pi_i\mathbf{u}\|_{\Omega_i} \le C\|\mathbf{u}\|_{r+1,\Omega_i}h^{r+1}, \quad 0\le r\le k+1$$

(see [22] and also [36, 24]). ∎

5. A posteriori estimates. We next derive several a posteriori error bounds, which depend only on the input data and the computed solution. The error estimators are utilized in an adaptive mesh refinement procedure to obtain the numerical solution on appropriate subdomain and mortar grids in the next section (see section 6.6).

In this section, we assume full H^2-regularity of the problem (1.1)–(1.3). We want to derive a posteriori estimates of the error functions

$$\xi = \mathbf{u} - \mathbf{u}_h, \quad \eta = p - p_h, \quad \text{and} \quad \delta = \lambda - \lambda_H. \tag{5.1}$$

5.1. Some saturation assumptions. It is shown in [46, 38] for RTN_0 ($k = 0$) rectangular elements with linear mortars and very general hanging interface nodes and mortar grid configurations satisfying (2.5) that

$$\sum_{\tau \in \mathcal{T}^{\Gamma,H}} \|\mu\|^2_{1/2,\tau} \le C d_H(\mu,\mu), \quad \mu \in M_H. \tag{5.2}$$

The proofs in [46, 38] can be generalized in a relatively straightforward way to the other mixed finite element spaces under consideration and to higher order elements.

The a priori error bounds from Theorems 4.1 and 4.4 motivate the following assumption on the mortar error.

Saturation Assumption 1. There exists a constant C such that

$$|||\lambda - \lambda_H||| := \left(\sum_{\tau \in \mathcal{T}^{\Gamma,H}} \sum_{E \in E_\tau} h_E^{-1} \|\lambda - \lambda_H\|^2_{\partial E \cap \tau} \right)^{1/2} \le C \|\mathbf{u} - \mathbf{u}_h\|. \tag{5.3}$$

For justification of (5.3), note that $|||\lambda - \lambda_H|||$ is closely related to the discrete $H^{1/2}(\Gamma)$ norm and, by (5.2), to $\|\lambda - \lambda_H\|_{d_H}$. Now, assuming that

$$\|\mathbf{u} - \mathbf{u}_h(\lambda)\| \le \gamma \|\mathbf{u} - \mathbf{u}_h\|,$$

which is reasonable, since $\mathbf{u}_h(\lambda)$ is the numerical solution based on the true interface data, we have, using (2.15),

$$\begin{aligned} C\|\lambda - \lambda_H\|_{d_H} &\le \|\mathbf{u}_h^*(\lambda) - \mathbf{u}_h^*(\lambda_H)\| = \|\mathbf{u}_h(\lambda) - \mathbf{u}_h(\lambda_H)\| = \|\mathbf{u}_h(\lambda) - \mathbf{u}_h\| \\ &\le \|\mathbf{u} - \mathbf{u}_h(\lambda)\| + \|\mathbf{u} - \mathbf{u}_h\| \le (1+\gamma)\|\mathbf{u} - \mathbf{u}_h\|. \end{aligned}$$

Let $\mathbf{V}_h'$, W_h', and M_H' be the finite element spaces of index one higher (i.e., of approximation order one more) than $\mathbf{V}_h$, W_h, and M_H, respectively. Let $\mathbf{u}_h' \in \mathbf{V}_h'$, $p_h' \in W_h'$, and $\lambda_H' \in M_H'$ be the mortar mixed finite element solution in these higher order spaces (see (2.6)–(2.8)). The a priori error estimates from Theorems 4.1 and 4.3 motivate the following assumption.

Saturation Assumption 2. There exist constants $\beta < 1$, $\beta_{\mathrm{div}} < 1$, and $C < \infty$ such that

$$\|\mathbf{u} - \mathbf{u}_h'\| \le \beta \|\mathbf{u} - \mathbf{u}_h\|, \tag{5.4}$$

$$\|\nabla \cdot (\mathbf{u} - \mathbf{u}_h')\| \le \beta_{\mathrm{div}} \|\nabla \cdot (\mathbf{u} - \mathbf{u}_h)\|, \tag{5.5}$$

$$\|p - p_h'\| \le C \|p - p_h\|. \tag{5.6}$$

Saturation assumptions are common in the literature regarding a posteriori results. They are justified by the a priori error theorems, Theorems 4.1, 4.3, and 4.4. The saturation assumptions merely state that the error *bounds* are asymptotically

close to the true error, and that h and H are sufficiently small, so that we can conclude that the higher order approximation is better than the lower order approximation. We need some assumption like this to guarantee that we have sufficient resolution that the coarse approximation contains some "reasonable" information about the solution, so that we can detect inadequate resolution.

5.2. Explicit residual-based estimators. We proceed in this subsection with the derivation of explicit residual-based upper and lower bounds on the error.

5.2.1. Upper bounds. Denote, for all $E \in \mathcal{T}_h$, $\tau \in \mathcal{T}^{\Gamma,H}$,

$$\omega_E^2 = \|K^{-1}\mathbf{u}_h + \nabla p_h\|_E^2 h_E^2 + \|f - \nabla \cdot \mathbf{u}_h\|_E^2 h_E^2 + \|\lambda_H - p_h\|_{\partial E \cap \Gamma}^2 h_E, \tag{5.7}$$

$$\omega_\tau^2 = \sum_{E \in E_\tau} \|[\mathbf{u}_h \cdot \nu]\|_{\partial E \cap \tau}^2 H_\tau^3, \tag{5.8}$$

where, for any $\mathbf{v} \in \mathbf{V}$, $\mathbf{v}|_{\Omega_i} = \mathbf{v}_i$,

$$[\mathbf{v} \cdot \nu]|_{\Gamma_{i,j}} = \mathbf{v}_i \cdot \nu_i + \mathbf{v}_j \cdot \nu_j$$

is the jump operator. We have an upper bound on the pressure error η.

THEOREM 5.1. *There exists a constant C, independent of h and H, such that*

$$\|\eta\|^2 \le C\Big\{ \sum_{E \in \mathcal{T}_h} \omega_E^2 + \sum_{\tau \in \mathcal{T}^{\Gamma,H}} \omega_\tau^2 + \sum_{e \in \mathcal{T}_h|_{\partial\Omega}} \|g - \mathcal{Q}_h g\|_e^2 h_e \Big\}. \tag{5.9}$$

Note that $\mathcal{Q}_h$ is applied on $\partial\Omega$, where it is single-valued. The proof of this theorem follows closely the proof of Theorem 3.1 in [44] with a straightforward modification of the argument to allow for the two scales h and H.

Remark 5.1. Due to the approximation property (3.9) of $\mathcal{Q}_h$, the last term in the bound of Theorem 5.1 is of higher order than the other terms. Therefore, its effect becomes negligible for small h.

The bound on ξ is expressed in terms of $h_E^{-1}\omega_E$ and $H_\tau^{-1}\omega_\tau$.

THEOREM 5.2. *Assume that the saturation assumptions* (5.3), (5.4), *and* (5.6) *hold. Then there exists a constant C, independent of β, h, and H, such that*

$$\|\xi\|_{H(\mathrm{div};\Omega)}^2 \le \frac{C}{(1-\beta)^2}\Big\{ \sum_{E \in \mathcal{T}_h} h_E^{-2}\omega_E^2 + \sum_{\tau \in \mathcal{T}^{\Gamma,H}} H_\tau^{-2}\omega_\tau^2 + \sum_{e \in \mathcal{T}_h|_{\partial\Omega}} \|g - \mathcal{Q}_h g\|_e^2 h_e^{-1} \Big\}.$$

The proof of this theorem follows closely the proof of Theorem 3.2 in [44] with a straightforward modification of the argument to allow for the two scales h and H.

5.2.2. Lower bounds. Next, we establish lower bounds on the error, which indicate that the residual error estimators can be used effectively in an adaptive mesh refinement algorithm.

THEOREM 5.3. *There exists a constant C, independent of h and H, such that*

$$\sum_{E \in \mathcal{T}_h} \omega_E^2 + \sum_{\tau \in \mathcal{T}^{\Gamma,H}} \omega_\tau^2 \le C\Big\{ \|\eta\|^2 + \sum_{E \in \mathcal{T}_h} h_E^2 \|\xi\|_{H(\mathrm{div};E)}^2 + \sum_{E \in \mathcal{T}_h} h_E \|\delta\|_{\partial E \cap \Gamma}^2 + \sum_{\tau \in \mathcal{T}^{\Gamma,H}} \sum_{E \in E_\tau} h_E^{-1} H_\tau^3 \|\xi\|_{H(\mathrm{div};E)}^2 \Big\}. \tag{5.10}$$

Moreover, the following local bounds hold for any $E \in \mathcal{T}_h$, $e \in \partial E$, and $\tau \in \mathcal{T}^{\Gamma,H}$:

$$\|K^{-1}\mathbf{u}_h + \nabla p_h\|_E^2 h_E^2 + \|f - \nabla\cdot\mathbf{u}_h\|_E^2 h_E^2 \le C(\|\eta\|_E^2 + \|\xi\|_{H(\mathrm{div};E)}^2 h_E^2), \tag{5.11}$$

$$\sum_{E\in E_\tau} \|[\mathbf{u}_h\cdot\nu]\|_{\partial E\cap\tau}^2 H_\tau^3 \le C \sum_{E\in E_\tau} h_E^{-1} H_\tau^3 \|\xi\|_{H(\mathrm{div};E)}^2, \tag{5.12}$$

$$\|\lambda_H - p_h\|_e^2 h_E \le C(\|\eta\|_E^2 + \|\xi\|_{H(\mathrm{div};E)}^2 h_E^2 + \|\delta\|_e^2 h_E). \tag{5.13}$$

The proof is a relatively straightforward modification of the proof of Theorem 3.3 in [44].

Remark 5.2. Generally, the terms after $\|\eta\|^2$ in (5.10) are of higher order. From Remarks 4.1 and 4.3, when $l = k$, the choice $H = \mathcal{O}(h^{(k+1)/(m+1/2)})$ gives optimal a priori errors of order $\mathcal{O}(h^{k+1})$ for p in L^2 and $\mathbf{u}$ in $H(\mathrm{div};\Omega)$, as well as for the mortar $\lambda = p$ in the d_H-norm (which bounds the L^2-norm). Thus, for C_1 and C_2 independent of h,

$$\begin{aligned} C_1\Big(\sum_{E\in\mathcal{T}_h}\omega_E^2 + \sum_{\tau\in\mathcal{T}^{\Gamma,H}}\omega_\tau^2 + \mathcal{O}(h^{2(k+1)+\alpha})\Big) \\ \le \|\eta\|^2 \le C_2\Big(\sum_{E\in\mathcal{T}_h}\omega_E^2 + \sum_{\tau\in\mathcal{T}^{\Gamma,H}}\omega_\tau^2 + \mathcal{O}(h^{2(k+1)+1})\Big), \end{aligned} \tag{5.14}$$

where $\alpha = \min\big(1, 3(k+1)/(m+1/2)-1\big)$. In the case of RTN_0 ($k=0$) and quadratic mortars ($m=2$), the optimal choice is $H = \mathcal{O}(h^{2/5})$, and $\alpha = 1/5 > 0$. Similarly, for linear mortars ($m=1$) with $H = \mathcal{O}(h^{2/3})$, $\alpha = 1 > 0$. Whenever $\alpha > 0$, the error in $\|\eta\|^2$ is dominated above and below by our local residual estimators $\sum_{E\in\mathcal{T}_h}\omega_E^2 + \sum_{\tau\in\mathcal{T}^{\Gamma,H}}\omega_\tau^2$ for small enough h, up to C_1 and C_2, and so this quantity is an efficient and reliable indicator of the pressure error.

5.3. Error estimators based on solving local problems. In this subsection, we develop an implicit error estimator which requires solving local (element) boundary value problems. These problems approximate the local residual equations satisfied by the true error. The motivation for considering implicit estimators comes from the unknown generic constants that appear in the explicit estimators. We show that the implicit estimator provides both optimal upper and lower bounds for the velocity error.

5.3.1. Global approximation to the error. Following the approach in [45], we first construct a global approximation to the error based on higher order finite element spaces. For $\mathbf{v}\in\mathbf{V}_i$, let

$$r(\mathbf{v}) = -\langle g, \mathbf{v}\cdot\nu\rangle_{\partial\Omega_i\setminus\Gamma} - (K^{-1}\mathbf{u}_h, \mathbf{v})_{\Omega_i} + (p_h, \nabla\cdot\mathbf{v})_{\Omega_i} - \langle\lambda_H, \mathbf{v}\cdot\nu_i\rangle_{\Gamma_i}. \tag{5.15}$$

Using (2.1)–(2.3), the true error satisfies the residual equations

$$(K^{-1}\xi, \mathbf{v})_{\Omega_i} - (\eta, \nabla\cdot\mathbf{v})_{\Omega_i} + \langle\delta, \mathbf{v}\cdot\nu_i\rangle_{\Gamma_i} = r(\mathbf{v}), \quad \mathbf{v}\in\mathbf{V}_i, \tag{5.16}$$

$$(\nabla\cdot\xi, w)_{\Omega_i} = (f - \nabla\cdot\mathbf{u}_h, w)_{\Omega_i}, \qquad w\in W_i, \tag{5.17}$$

$$\sum_{i=1}^n \langle\xi\cdot\nu_i, \mu\rangle_{\Gamma_i} = -\sum_{i=1}^n \langle\mathbf{u}_h\cdot\nu_i, \mu\rangle_{\Gamma_i}, \qquad \mu\in M. \tag{5.18}$$

Recall from the previous subsection that $\mathbf{V}_h' \times W_h' \times M_H'$ is the mortar mixed finite element space of index order one higher than $\mathbf{V}_h \times W_h \times M_H$. Let

$$\xi' = \mathbf{u}_h' - \mathbf{u}_h, \quad \eta' = p_h' - p_h, \quad \text{and} \quad \delta' = \lambda_H' - \lambda_H. \tag{5.19}$$

Then $(\xi', \eta', \delta') \in \mathbf{V}_h' \times W_h' \times M_H'$ is the finite element approximation to (ξ, η, δ) satisfying

$$(K^{-1}\xi', \mathbf{v})_{\Omega_i} - (\eta', \nabla \cdot \mathbf{v})_{\Omega_i} + \langle \delta', \mathbf{v} \cdot \nu_i \rangle_{\Gamma_i} = r(\mathbf{v}), \quad \mathbf{v} \in \mathbf{V}_{h,i}', \tag{5.20}$$

$$(\nabla \cdot \xi', w)_{\Omega_i} = (f - \nabla \cdot \mathbf{u}_h, w)_{\Omega_i}, \qquad w \in W_{h,i}', \tag{5.21}$$

$$\sum_{i=1}^{n} \langle \xi' \cdot \nu_i, \mu \rangle_{\Gamma_i} = -\sum_{i=1}^{n} \langle \mathbf{u}_h \cdot \nu_i, \mu \rangle_{\Gamma_i}, \qquad \mu \in M_H'. \tag{5.22}$$

The saturation assumptions (5.4) and (5.5) imply

$$\frac{1}{1+\beta}\|\xi'\| \le \|\xi\| \le \frac{1}{1-\beta}\|\xi'\|, \tag{5.23}$$

$$\frac{1}{1+\beta_{\mathrm{div}}}\|\nabla \cdot \xi'\| \le \|\nabla \cdot \xi\| \le \frac{1}{1-\beta_{\mathrm{div}}}\|\nabla \cdot \xi'\|, \tag{5.24}$$

and so it is enough to estimate ξ', since we do not wish to compute $\mathbf{u}_h'$.

5.3.2. Local (element) approximation to the error. For any $E \in \mathcal{T}_h$, the true error satisfies the local equations

$$(K^{-1}\xi, \mathbf{v})_E - (\eta, \nabla \cdot \mathbf{v})_E = r_E(\mathbf{v}) - \langle p, \mathbf{v} \cdot \nu_E \rangle_{\partial E}, \quad \mathbf{v} \in \mathbf{V}(E), \tag{5.25}$$

$$(\nabla \cdot \xi, w)_E = (f - \nabla \cdot \mathbf{u}_h, w)_E, \quad w \in W(E), \tag{5.26}$$

where

$$r_E(\mathbf{v}) = -(K^{-1}\mathbf{u}_h, \mathbf{v})_E + (p_h, \nabla \cdot \mathbf{v})_E. \tag{5.27}$$

We construct a higher order local approximation of the error by solving element subproblems: Find $\psi' \in \mathbf{V}_h'(E)$ and $\theta' \in W_h'(E)$ such that

$$(K^{-1}\psi', \mathbf{v})_E - (\theta', \nabla \cdot \mathbf{v})_E = r_E(\mathbf{v}) - \langle p_A, \mathbf{v} \cdot \nu_E \rangle_{\partial E}, \quad \mathbf{v} \in \mathbf{V}_h'(E), \tag{5.28}$$

$$(\nabla \cdot \psi', w)_E = (f - \nabla \cdot \mathbf{u}_h, w)_E, \quad w \in W_h'(E), \tag{5.29}$$

where $p_A = g$ on $\partial\Omega$, $p_A = \lambda_H$ on $\partial E \cap \Gamma$, and $p_A = \tilde{p}_h$ on $\partial E \cap \mathcal{E}_h$, where $\tilde{p}_h \in \Lambda_h(\partial E) = \mathbf{V}_h(E) \cdot \nu$ is the Lagrange multiplier for $\mathbf{V}_h$ and W_h in the standard hybrid formulation of the mixed method [10, 16], which can be defined from $\mathbf{u}_h$ and p_h as

$$\langle \tilde{p}_h, \mathbf{v} \cdot \nu_E \rangle_{\partial E} = -(K^{-1}\mathbf{u}_h, \mathbf{v})_E + (p_h, \nabla \cdot \mathbf{v})_E, \quad \mathbf{v} \in \mathbf{V}_h(E). \tag{5.30}$$

Note that (2.6) implies that $\tilde{p}_h$ is single-valued on $\mathcal{E}_h$. Let $\tilde{p}'$ be the Lagrange multiplier for the higher order spaces $\mathbf{V}_h'$ and W_h' satisfying

$$\langle \tilde{p}', \mathbf{v} \cdot \nu_E \rangle_{\partial E} = -(K^{-1}\mathbf{u}_h', \mathbf{v})_E + (p_h', \nabla \cdot \mathbf{v})_E, \quad \mathbf{v} \in V_h'(E). \tag{5.31}$$

Again, $\tilde{p}'$ is single-valued on $\mathcal{E}_h$.

We need one last saturation assumption.

Saturation Assumption 3. There exists a constant C such that

$$\left(\sum_{e \in \mathcal{E}_h} h_e^{-1} \|\tilde{p}' - \tilde{p}_h\|_e^2 \right)^{1/2} \le C\|\mathbf{u} - \mathbf{u}_h\|. \tag{5.32}$$

The assumption (5.32) is motivated by the a priori error estimate for the Lagrange multiplier [16]

$$\Big(\sum_{e\in\mathcal{E}_h} h_e^{-1} \|\bar{p} - \tilde{p}_h\|_e^2 \Big)^{1/2} \le C h^{k+1},$$

where $\bar{p}$ is the L^2-projection of p onto $\mathbf{V}_h \cdot \nu|_{\mathcal{E}_h}$.

THEOREM 5.4. *If the saturation assumptions* (5.3), (5.4), (5.5), *and* (5.32) *hold, then there exist constants C_1 and C_2, independent of β and $\beta_{\rm div}$, such that*

$$\begin{aligned} C_1 \Big[\|\psi'\|_{H(\mathrm{div};\Omega)} + \Big(\sum_{\tau\in\mathcal{T}^{\Gamma,H}} \sum_{E\in E_\tau} \|[\mathbf{u}_h\cdot\nu]\|^2_{\partial E\cap\tau} h_E \Big)^{1/2} \Big] &\le \|\xi\|_{H(\mathrm{div};\Omega)} \\ \le \frac{C_2}{(1-\beta_{\max})^2} \Big[\|\psi'\|_{H(\mathrm{div};\Omega)} + \Big(\sum_{\tau\in\mathcal{T}^{\Gamma,H}} \sum_{E\in E_\tau} \|[\mathbf{u}_h\cdot\nu]\|^2_{\partial E\cap\tau} h_E \Big)^{1/2} \Big], \end{aligned} \tag{5.33}$$

where $\beta_{\max} = \max\{\beta, \beta_{\rm div}\}$.

The proof is similar to the proof of Theorem 4.1 in [44] but differs in the technical details in handling the two scales. We reproduce the proof here for completeness.

Proof. Due to (5.21) and (5.29), it holds on every $E \in \mathcal{T}_h$ that

$$\nabla\cdot\psi' = \nabla\cdot\xi'. \tag{5.34}$$

Next, the sum over all elements in (5.28) with $\mathbf{v} = \psi' - \xi'$ gives

$$\begin{aligned} &\sum_{E\in\mathcal{T}_h} \big[(K^{-1}(\psi'-\xi'), \psi'-\xi')_E - (\theta'-\eta', \nabla\cdot(\psi'-\xi'))_E \big] \\ &\quad = \sum_{E\in\mathcal{T}_h} \big[-(K^{-1}\xi', \psi'-\xi')_E + (\eta', \nabla\cdot(\psi'-\xi'))_E \\ &\qquad\qquad + r_E(\psi'-\xi') - \langle p_A, (\psi'-\xi')\cdot\nu_E\rangle_{\partial E} \big] \\ &\quad = \sum_{E\in\mathcal{T}_h} \big[-(K^{-1}\mathbf{u}_h', \psi'-\xi')_E + (p_h', \nabla\cdot(\psi'-\xi'))_E - \langle \tilde{p}_h, (\psi'-\xi')\cdot\nu_E\rangle_{\partial E\cap\mathcal{E}_h} \\ &\qquad\qquad - \langle g, (\psi'-\xi')\cdot\nu\rangle_{\partial E\cap\partial\Omega} - \langle \lambda_H, (\psi'-\xi')\cdot\nu_E\rangle_{\partial E\cap\Gamma} \big] \\ &\quad = \sum_{E\in\mathcal{T}_h} \big[\langle \tilde{p}' - \tilde{p}_h, (\psi'-\xi')\cdot\nu_E\rangle_{\partial E\cap\mathcal{E}_h} + \langle \lambda_H' - \lambda_H, (\psi'-\xi')\cdot\nu_E\rangle_{\partial E\cap\Gamma} \big], \end{aligned} \tag{5.35}$$

wherein for the last equality we have used (5.31) and (2.6) for the higher order (primed) spaces to see that $\tilde{p}'$ is the projection of g onto $\partial\Omega$ and the projection of λ_H' onto Γ. The first term on the right-hand side can be bounded as

$$\begin{aligned} &\Big| \sum_{E\in\mathcal{T}_h} \langle \tilde{p}' - \tilde{p}_h, (\psi'-\xi')\cdot\nu_E\rangle_{\partial E\cap\mathcal{E}_h} \Big| \\ &\qquad \le \sum_{e\in\mathcal{E}_h} h_e^{-1/2} \|\tilde{p}' - \tilde{p}_h\|_e h_e^{1/2} \|(\psi'-\xi')\cdot\nu_e\|_e \\ &\qquad \le C\|\xi\| \|\psi'-\xi'\| \end{aligned} \tag{5.36}$$

using the saturation assumption (5.32) and the well-known local trace inequality akin to (3.18):

$$\forall\, E \in \mathcal{T}_h,\ e \in \partial E, \quad \|\mathbf{v}\cdot\nu\|_e \le C h_E^{-1/2}\|\mathbf{v}\|_E \quad \forall\, \mathbf{v} \in \mathbf{V}_h. \tag{5.37}$$

For the second term on the right-hand side in (5.35), we have

$$\begin{aligned}\left|\sum_{E\in\mathcal{T}_h}\langle\lambda_H'-\lambda_H,(\psi'-\xi')\cdot\nu_E\rangle_{\partial E\cap\Gamma}\right| &= \left|\sum_{i=1}^{n}\langle\delta',(\psi'-\xi')\cdot\nu_i\rangle_{\Gamma_i}\right| \\ &\le \sum_{\tau\in\mathcal{T}^{\Gamma,h}}\sum_{E\in E_\tau} h_E^{-1/2}\|\delta'\|_{\partial E\cap\tau}h_E^{1/2}\|[(\psi'-\xi')\cdot\nu]\|_{\partial E\cap\tau} \\ &\le |||\delta'|||\,\|\psi'-\xi'\| \\ &\le C\|\xi\|\|\psi'-\xi'\|,\end{aligned} \tag{5.38}$$

where we have used (5.37), (5.3), and (5.4) in the last two inequalities.

A combination of (5.34)–(5.38) implies that

$$\|\psi'-\xi'\| \le C\|\xi\|,$$

and therefore

$$\|\psi'\| \le C\|\xi\|, \tag{5.39}$$

using (5.23). The divergence bound

$$\|\nabla\cdot\psi'\| \le \|\nabla\cdot\xi\|$$

follows from (5.29) with $w = \nabla\cdot\psi'$, since $f - \nabla\cdot\mathbf{u}_h = \nabla\cdot\xi$. Therefore,

$$\|\psi'\|_{H(\mathrm{div};\Omega)} \le C\|\xi\|_{H(\mathrm{div};\Omega)}. \tag{5.40}$$

This with (5.12) completes the proof of the left inequality in (5.33).

For the right inequality in (5.33), from (5.35), we have (with (5.34)) that

$$\begin{aligned}&(K^{-1}(\psi'-\xi'),\psi'-\xi') \\ &\quad= \sum_{E\in\mathcal{T}_h}\left[\langle\tilde{p}'-\tilde{p}_h,(\psi'-\xi')\cdot\nu_E\rangle_{\partial E\cap\mathcal{E}_h} + \langle\lambda_H'-\lambda_H,(\psi'-\xi')\cdot\nu_E\rangle_{\partial E\cap\Gamma}\right] \\ &\quad= -\sum_i\langle\delta',\xi'\cdot\nu_i\rangle_{\Gamma_i} - \sum_{E\in\mathcal{T}_h}\left[\langle\tilde{p}'-\tilde{p}_h,\psi'\cdot\nu_E\rangle_{\partial E\cap\mathcal{E}_h} + \langle\lambda_H'-\lambda_H,\psi'\cdot\nu_E\rangle_{\partial E\cap\Gamma}\right].\end{aligned} \tag{5.41}$$

Using (5.22), for any $\epsilon > 0$, the first term on the right-hand side can be bounded as

$$\begin{aligned}\left|\sum_{i=1}^{n}\langle\delta',\xi'\cdot\nu_i\rangle_{\Gamma_i}\right| &= \left|\sum_{i=1}^{n}\langle\delta',\mathbf{u}_h\cdot\nu_i\rangle_{\Gamma_i}\right| \\ &\le \sum_{\tau\in\mathcal{T}^{\Gamma,h}}\sum_{E\in E_\tau} h_E^{-1/2}\|\delta'\|_{\partial E\cap\tau}h_E^{1/2}\|[\mathbf{u}_h\cdot\nu]\|_{\partial E\cap\tau} \\ &\le \epsilon\|\xi\|^2 + C\epsilon^{-1}\sum_{\tau\in\mathcal{T}^{\Gamma,h}}\sum_{E\in E_\tau}\|[\mathbf{u}_h\cdot\nu]\|^2_{\partial E\cap\tau}h_E,\end{aligned} \tag{5.42}$$

where we have used (5.3) and (5.4) in the last inequality. For the last two terms on the right-hand side in (5.41), arguments similar to (5.36) and (5.38) give

$$\left|\sum_{E\in\mathcal{T}_h}\left[\langle\tilde{p}'-\tilde{p}_h,\psi'\cdot\nu_E\rangle_{\partial E\cap\mathcal{E}_h}+\langle\lambda'_H-\lambda_H,\psi'\cdot\nu_E\rangle_{\partial E\cap\Gamma}\right]\right| \le \epsilon\|\xi\|^2+C\epsilon^{-1}\|\psi'\|^2. \tag{5.43}$$

Combining (5.41)–(5.43), using the triangle inequality and (5.23), and taking ϵ proportional to $(1-\beta)^2$, we obtain

$$\|\xi\|\le\frac{C}{(1-\beta)^2}\left[\|\psi'\|+\left(\sum_{\tau\in\mathcal{T}^{\Gamma,h}}\sum_{E\in E_\tau}\|[\mathbf{u}_h\cdot\nu]\|^2_{\partial E\cap\tau}h_E\right)^{1/2}\right].$$

An application of (5.24) and (5.34) completes the proof. ∎

6. Numerical results. In this section, we present several numerical tests confirming the theoretical convergence rates and illustrating the behavior of the method. The examples are on the unit square (cube for Example 3) and use the lowest order RTN spaces [39, 37], RTN_0, on rectangles (for which $k=l=0$). The boundary conditions are Dirichlet on the left and right edges and Neumann on the rest of the boundary. Unless otherwise noted, the domain is divided into four (eight for Example 3) subdomains with interfaces along the $x=1/2$ and $y=1/2$ (and $z=1/2$ for Example 3) lines.

We employ the nonoverlapping domain decomposition algorithm from section 2.2 for the solution of the algebraic problem. In particular, we employ the CG method for solving the symmetric and positive definite interface coarse scale mortar problem (2.13), which results from the multiscale algebraic system. The balancing preconditioner [20, 38] is used for accelerating the convergence of the CG iteration. As a result, both the condition number of the interface problem and the number of interface iterations grow only very slowly when increasing the dimension of the mortar problem, either through refining the mortar grid or through increasing the number of subdomains. In the numerical experiments, we report the rates of convergence of the numerical solution to the true solution, as well as the number of interface iterations and estimated condition number. In some cases, see Tables 6.4 and 6.8, the condition number is larger on the coarsest grid than on the finer grids. This is due to an underestimation of the smallest eigenvalue on the coarsest grid.

The convergence rates are established by running each test case on several levels of grid refinement and computing a least squares fit to the error. We consider both matching and nonmatching initial grids. For initial matching grids, we use a 2×2 ($2\times 2\times 2$ for Example 3) subdomain grid (so, initially, $h=1/4$). For initial nonmatching grids, we use 2×2 or 3×3 subdomain grids alternated in a checkerboard fashion. We test both continuous and discontinuous quadratic mortars ($m=2$) and compare the results to the cases of linear mortars ($m=1$), continuous or discontinuous, respectively. The initial mortar grids on all interfaces have one element (so, initially, $H=1/2$). For the case of quadratic mortars, on each level of grid refinement we divide each subdomain element diameter h by four and halve each mortar element diameter H so that $H=h^{1/2}$ (see Remarks 4.1–4.3). For the case of linear mortars, we halve both subdomain and mortar element diameters, and so $H=2h$ on each level.

TABLE 6.1
Theoretical convergence rates for quadratic and linear mortars.

m	H	$\|\|p-p_h\|\|$	$\|\|\mathbf{u}-\mathbf{u}_h\|\|$	$\|\|\|p-p_h\|\|\|$	$\|\|\|\mathbf{u}-\mathbf{u}_h\|\|\|$	$\|\|\|p-\lambda_H\|\|\|$	
						Full K	diag K
2	$h^{1/2}$	1	1	1.5	1.25	1.25	1.5
1	$2h$	1	1	2	1.5	1.5	2

TABLE 6.2
Number of iterations, condition number, discrete norm errors, and convergence rates for Example 1: *continuous quadratic mortars and matching grids.*

$1/h$	Iter.	Cond.	$\|\|p-p_h\|\|$	$\|\|\mathbf{u}-\mathbf{u}_h\|\|$	$\|\|\|p-p_h\|\|\|$	$\|\|\|\mathbf{u}-\mathbf{u}_h\|\|\|$	$\|\|\|p-\lambda_H\|\|\|$
4	4	1.20E+0	3.38E-1	3.00E-1	6.87E-2	2.13E-2	5.81E-2
16	12	2.37E+1	7.98E-2	6.93E-2	4.21E-3	1.89E-3	3.50E-3
64	14	2.17E+1	1.99E-2	1.72E-2	2.59E-4	1.97E-4	2.17E-4
256	16	2.73E+1	4.97E-3	4.31E-3	1.61E-5	2.43E-5	1.37E-5
Rate			$\mathcal{O}(h^{1.01})$	$\mathcal{O}(h^{1.02})$	$\mathcal{O}(h^{2.01})$	$\mathcal{O}(h^{1.63})$	$\mathcal{O}(h^{2.01})$

For each test case, we report on some of the possible combinations between mortar types (continuous or discontinuous) and grid types (matching or nonmatching). The results for the rest of the combinations are similar.

The theoretical convergence rates for the above choices of subdomain and mortar grids are given in Table 6.1. The second pressure error in the tables, $|||p-p_h|||$, is the discrete L^2-norm induced by the midpoint rule on $\mathcal{T}_h$, which is $\mathcal{O}(h^2)$-close to $\|\hat{p}-p_h\|$. The discrete velocity error $|||\mathbf{u}-\mathbf{u}_h|||$ is defined in (4.6) above. The discrete interface pressure error $|||p-\lambda_H|||$ is computed by adding for each block Ω_i the discrete L^2-norm of $p-\mathcal{Q}_{h,i}\lambda_H$ induced by the midpoint rule on the traces of $\mathcal{T}_{h,i}$ on $\partial\Omega_i\cap\Gamma$. This is essentially the L^2-norm, and we expect it to be $1/2$ power of H better than $\|p-\lambda_H\|_{d_H}$, since the latter is essentially $\|p-\lambda_H\|_{H^{1/2}(\Gamma)}$ (see [20], [46], and Remark 6.1 in [5]).

6.1. Example 1. In the first example, we solve a problem with known analytic solution

$$p(x,y)=x^3y^4+x^2+\sin(xy)\cos(y)$$

and full tensor coefficient

$$K=\begin{pmatrix}(x+1)^2+y^2 & \sin(xy)\\ \sin(xy) & (x+1)^2\end{pmatrix}.$$

Convergence rates, the number of interface iterations, and the condition number of the interface operator for this test case are given in Tables 6.2–6.5. We observe that the convergence rates are at least as good as predicted by the theory. For all four cases, we obtain optimal order $\mathcal{O}(h)$ for both the pressure and the velocity L^2-error.

The discrete pressure error $|||p-p_h||| \approx \|\hat{p}-p_h\|$ is superconvergent of order $\mathcal{O}(h^2)$ for both quadratic and linear mortars, even though Theorem 4.3 predicts only $\mathcal{O}(h^{3/2})$ for quadratic mortars. By Theorem 4.2, the discrete velocity error $|||\mathbf{u}-\mathbf{u}_h|||$ is superconvergent of order $\mathcal{O}(h^{5/4})$ for quadratic mortars and $\mathcal{O}(h^{3/2})$ for linear mortars. Again, we observe higher than expected superconvergence for the case of quadratic mortars. Last, the discrete interface pressure error $|||p-\lambda_H||| \approx H^{1/2}\|p-\lambda_H\|_{d_H}$ is also better than expected, achieving convergence of $\mathcal{O}(h^2)$.

TABLE 6.3
Number of iterations, condition number, discrete norm errors, and convergence rates for Example 1: *continuous linear mortars and matching grids.*

$1/h$	Iter.	Cond.	$\|\|p-p_h\|\|$	$\|\|\mathbf{u}-\mathbf{u}_h\|\|$	$\|\|\|p-p_h\|\|\|$	$\|\|\|\mathbf{u}-\mathbf{u}_h\|\|\|$	$\|\|\|p-\lambda_H\|\|\|$
4	4	2.44E+0	3.38E-1	3.00E-1	6.87E-2	2.13E-2	5.81E-2
8	7	9.91E+0	1.62E-1	1.41E-1	1.70E-2	6.33E-3	1.41E-2
16	13	2.38E+1	7.98E-2	6.93E-2	4.21E-3	1.88E-3	3.50E-3
32	19	3.48E+1	3.98E-2	3.45E-2	1.04E-3	5.88E-4	8.67E-4
64	23	4.40E+1	1.99E-2	1.72E-2	2.59E-4	1.93E-4	2.16E-4
128	23	5.54E+1	9.94E-3	8.62E-3	6.46E-5	6.53E-5	5.38E-5
256	23	6.76E+1	4.97E-3	4.31E-3	1.61E-5	2.27E-5	1.35E-5
Rate			$\mathcal{O}(h^{1.01})$	$\mathcal{O}(h^{1.02})$	$\mathcal{O}(h^{2.01})$	$\mathcal{O}(h^{1.65})$	$\mathcal{O}(h^{2.01})$

TABLE 6.4
Number of iterations, condition number, discrete norm errors, and convergence rates for Example 1: *discontinuous quadratic mortars and nonmatching grids.*

$1/h$	Iter.	Cond.	$\|\|p-p_h\|\|$	$\|\|\mathbf{u}-\mathbf{u}_h\|\|$	$\|\|\|p-p_h\|\|\|$	$\|\|\|\mathbf{u}-\mathbf{u}_h\|\|\|$	$\|\|\|p-\lambda_H\|\|\|$
4	8	1.88E+1	2.64E-1	2.03E-1	4.62E-2	2.13E-2	4.45E-2
16	7	2.45E+0	6.37E-2	4.86E-2	2.83E-3	1.82E-3	2.72E-3
64	7	2.34E+0	1.59E-2	1.21E-2	1.75E-4	1.59E-4	1.69E-4
256	8	3.03E+0	3.98E-3	3.03E-3	1.09E-5	1.68E-5	1.06E-5
Rate			$\mathcal{O}(h^{1.01})$	$\mathcal{O}(h^{1.01})$	$\mathcal{O}(h^{2.01})$	$\mathcal{O}(h^{1.72})$	$\mathcal{O}(h^{2.01})$

TABLE 6.5
Number of iterations, condition number, discrete norm errors, and convergence rates for Example 1: *discontinuous linear mortars and nonmatching grids.*

$1/h$	Iter.	Cond.	$\|\|p-p_h\|\|$	$\|\|\mathbf{u}-\mathbf{u}_h\|\|$	$\|\|\|p-p_h\|\|\|$	$\|\|\|\mathbf{u}-\mathbf{u}_h\|\|\|$	$\|\|\|p-\lambda_H\|\|\|$
4	4	1.31E+0	2.63E-1	2.04E-1	4.54E-2	2.35E-2	4.55E-2
8	7	1.79E+0	1.28E-1	9.82E-2	1.14E-2	7.44E-3	1.14E-2
16	7	2.12E+0	6.37E-2	4.86E-2	2.82E-3	2.30E-3	2.86E-3
32	7	2.61E+0	3.18E-2	2.43E-2	7.01E-4	7.29E-4	7.13E-4
64	8	3.27E+0	1.59E-2	1.21E-2	1.75E-4	2.38E-4	1.78E-4
128	8	4.08E+0	7.95E-3	6.06E-3	4.36E-5	7.99E-5	4.45E-5
256	8	5.02E+0	3.98E-3	3.03E-3	1.09E-5	2.74E-5	1.11E-5
Rate			$\mathcal{O}(h^{1.01})$	$\mathcal{O}(h^{1.01})$	$\mathcal{O}(h^{2.01})$	$\mathcal{O}(h^{1.63})$	$\mathcal{O}(h^{2.00})$

Based on comparing the results from linear and quadratic mortars, we observe that in certain cases for fine meshes the quadratic mortars are more efficient: we achieve the same accuracy with less computational work. For example, in the case of continuous mortars, for the finest level of grid refinement, the accuracy is comparable, but there is more than a 30% reduction in the number of interface problem iterations needed for quadratic mortars (see the lines for $1/h = 256$ in Tables 6.2 and 6.3). In the case of discontinuous mortars, both linear and quadratic mortars are very efficient, with the number of interface iterations remaining almost unchanged with the grid refinement. We will see from Example 5 below that for heterogeneous problems with large variations in the velocity, discontinuous quadratic mortars outperform discontinuous linear mortars.

The computed pressure and velocity with discontinuous quadratic and linear mortars on the same nonmatching subdomain grids (first/second level of refinement for quadratic/linear mortars) are shown in Figure 6.1. Although the two solutions look the same, the velocity error along the interfaces is somewhat larger for the case of linear mortars, as can be seen in Figure 6.2, where the magnified numerical error is shown.

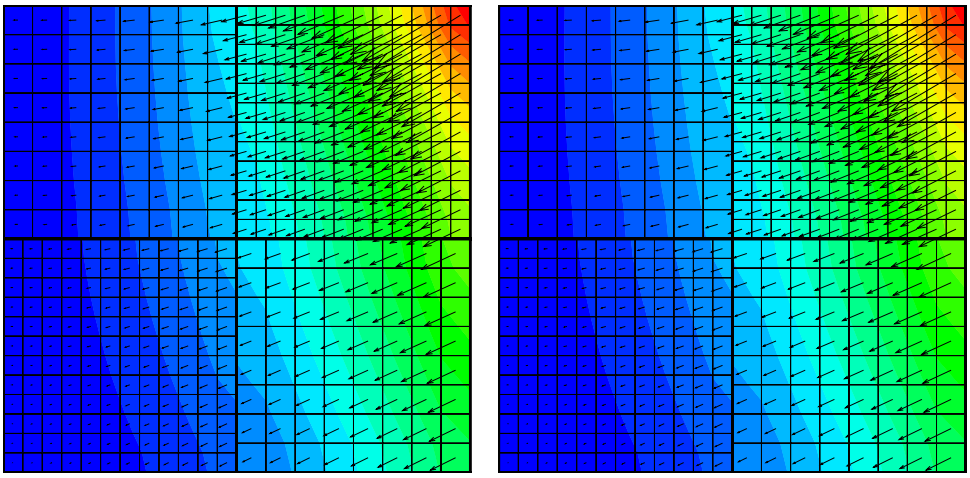

(a) *Discontinuous quadratic mortars* (b) *Discontinuous linear mortars*

FIG. 6.1. *Computed pressure (shade) and velocity (arrows) for Example* 1 *on nonmatching grids.*

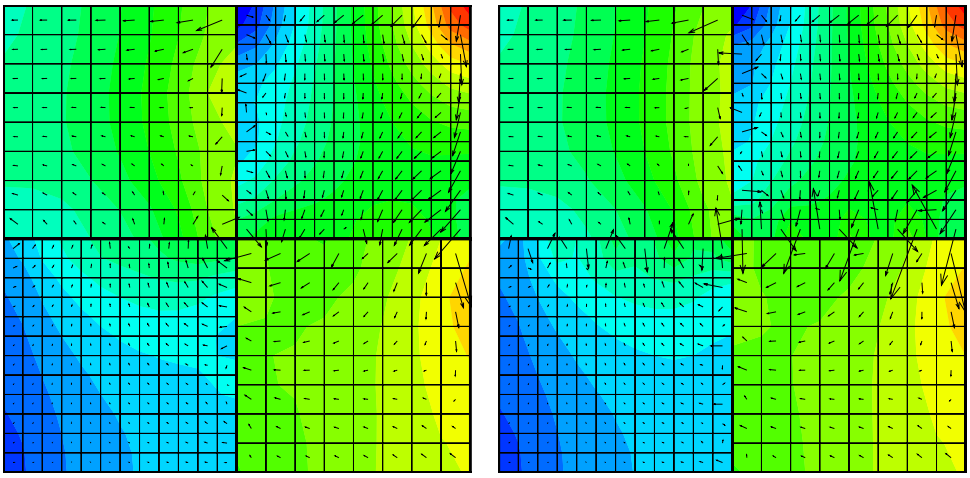

(a) *Discontinuous quadratic mortars* (b) *Discontinuous linear mortars*

FIG. 6.2. *Error in pressure (shade) and velocity (arrows) for Example* 1 *on nonmatching grids.*

6.2. Example 2. In the second example, we test a problem with a discontinuous coefficient. We choose $K = I$ for $0 \le x < 1/2$ and $K = 10I$ for $1/2 < x \le 1$. The solution

$$p(x,y) = \begin{cases} x^2y^3 + \cos(xy), & 0 \le x \le 1/2, \\ \left(\frac{2x+9}{20}\right)^2 y^3 + \cos\left(\frac{2x+9}{20}y\right), & 1/2 \le x \le 1, \end{cases}$$

is chosen to be continuous and have continuous normal flux at $x = 1/2$. Convergence rates are given in Tables 6.6–6.9. Again, they agree with the theory, even though K is mildly discontinuous.

TABLE 6.6
Number of iterations, condition number, discrete norm errors, and convergence rates for Example 2: *discontinuous quadratic mortars and matching grids.*

$1/h$	Iter.	Cond.	$\|\|p-p_h\|\|$	$\|\|\mathbf{u}-\mathbf{u}_h\|\|$	$\|\|\|p-p_h\|\|\|$	$\|\|\|\mathbf{u}-\mathbf{u}_h\|\|\|$	$\|\|\|p-\lambda_H\|\|\|$
4	5	1.83E+0	2.35E-2	8.17E-2	1.51E-3	6.77E-2	4.58E-3
16	8	3.91E+0	5.69E-3	1.95E-2	1.06E-4	4.46E-3	2.98E-4
64	6	3.74E+0	1.42E-3	4.87E-3	6.76E-6	4.53E-4	2.20E-5
256	7	4.88E+0	3.55E-4	1.22E-3	4.34E-7	8.70E-5	2.14E-6
Rate			$\mathcal{O}(h^{1.01})$	$\mathcal{O}(h^{1.01})$	$\mathcal{O}(h^{1.96})$	$\mathcal{O}(h^{1.61})$	$\mathcal{O}(h^{1.85})$

TABLE 6.7
Number of iterations, condition number, discrete norm errors, and convergence rates for Example 2: *discontinuous linear mortars and matching grids.*

$1/h$	Iter.	Cond.	$\|\|p-p_h\|\|$	$\|\|\mathbf{u}-\mathbf{u}_h\|\|$	$\|\|\|p-p_h\|\|\|$	$\|\|\|\mathbf{u}-\mathbf{u}_h\|\|\|$	$\|\|\|p-\lambda_H\|\|\|$
4	5	1.83E+0	2.35E-2	8.17E-2	1.51E-3	6.77E-2	4.58E-3
8	7	2.62E+0	1.15E-2	3.94E-2	4.15E-4	1.73E-2	1.16E-3
16	7	3.50E+0	5.69E-3	1.95E-2	1.06E-4	4.37E-3	2.92E-4
32	7	4.55E+0	2.84E-3	9.71E-3	2.68E-5	1.10E-3	7.31E-5
64	7	5.75E+0	1.42E-3	4.85E-3	6.71E-6	2.74E-4	1.83E-5
128	7	7.11E+0	7.10E-4	2.42E-3	1.68E-6	6.86E-5	4.58E-6
256	8	8.63E+0	3.55E-4	1.21E-3	4.21E-7	1.72E-5	1.14E-6
Rate			$\mathcal{O}(h^{1.01})$	$\mathcal{O}(h^{1.01})$	$\mathcal{O}(h^{1.98})$	$\mathcal{O}(h^{1.99})$	$\mathcal{O}(h^{2.00})$

TABLE 6.8
Number of iterations, condition number, discrete norm errors, and convergence rates for Example 2: *continuous quadratic mortars and nonmatching grids.*

$1/h$	Iter.	Cond.	$\|\|p-p_h\|\|$	$\|\|\mathbf{u}-\mathbf{u}_h\|\|$	$\|\|\|p-p_h\|\|\|$	$\|\|\|\mathbf{u}-\mathbf{u}_h\|\|\|$	$\|\|\|p-\lambda_H\|\|\|$
4	9	1.11E+2	1.84E-2	6.20E-2	1.13E-3	4.58E-2	3.27E-3
16	14	2.55E+1	4.37E-3	1.50E-2	8.07E-5	3.67E-3	2.40E-4
64	15	2.41E+1	1.09E-3	3.73E-3	5.37E-6	6.45E-4	2.45E-5
256	16	3.03E+1	2.72E-4	9.26E-4	3.70E-7	1.27E-4	2.97E-6
Rate			$\mathcal{O}(h^{1.01})$	$\mathcal{O}(h^{1.01})$	$\mathcal{O}(h^{1.93})$	$\mathcal{O}(h^{1.40})$	$\mathcal{O}(h^{1.68})$

TABLE 6.9
Number of iterations, condition number, discrete norm errors, and convergence rates for Example 2: *continuous linear mortars and nonmatching grids.*

$1/h$	Iter.	Cond.	$\|\|p-p_h\|\|$	$\|\|\mathbf{u}-\mathbf{u}_h\|\|$	$\|\|\|p-p_h\|\|\|$	$\|\|\|\mathbf{u}-\mathbf{u}_h\|\|\|$	$\|\|\|p-\lambda_H\|\|\|$
4	5	1.68E+1	1.84E-2	9.57E-2	1.28E-3	7.04E-2	5.23E-3
8	8	1.70E+1	8.83E-3	4.05E-2	3.29E-4	2.38E-2	1.45E-3
16	14	2.55E+1	4.37E-3	1.75E-2	8.20E-5	7.76E-3	3.53E-4
32	22	3.73E+1	2.18E-3	8.06E-3	2.05E-5	2.62E-3	8.75E-5
64	22	4.32E+1	1.09E-3	3.85E-3	5.10E-6	9.06E-4	2.18E-5
128	24	5.26E+1	5.44E-4	1.88E-3	1.27E-6	3.17E-4	5.46E-6
256	23	6.26E+1	2.72E-4	9.28E-4	3.19E-7	1.11E-4	1.36E-6
Rate			$\mathcal{O}(h^{1.01})$	$\mathcal{O}(h^{1.11})$	$\mathcal{O}(h^{2.00})$	$\mathcal{O}(h^{1.55})$	$\mathcal{O}(h^{1.99})$

6.3. Example 3. In the third example, we test a three-dimensional problem with known analytic solution

$$p(x,y,z) = x + y + z - 1.5$$

and full tensor coefficient

$$K = \begin{pmatrix} x^2+y^2+1 & 0 & 0 \\ 0 & z^2+1 & \sin(xy) \\ 0 & \sin(xy) & x^2y^2+1 \end{pmatrix}.$$

TABLE 6.10
Number of iterations, condition number, discrete norm errors, and convergence rates for Example 3: *discontinuous quadratic mortars and matching grids.*

$1/h$	Iter.	Cond.	$\|\|p-p_h\|\|$	$\|\|\mathbf{u}-\mathbf{u}_h\|\|$	$\|\|\|p-p_h\|\|\|$	$\|\|\|\mathbf{u}-\mathbf{u}_h\|\|\|$	$\|\|\|p-\lambda_H\|\|\|$
4	10	3.38E+0	4.33E-1	1.01E-1	1.87E-2	3.27E-3	1.42E-2
16	15	9.70E+0	1.08E-1	2.52E-2	1.09E-3	4.60E-4	8.38E-4
64	14	5.15E+0	2.71E-2	6.29E-3	6.69E-5	5.58E-5	5.17E-5
Rate			$\mathcal{O}(h^{1.00})$	$\mathcal{O}(h^{1.00})$	$\mathcal{O}(h^{2.03})$	$\mathcal{O}(h^{1.47})$	$\mathcal{O}(h^{2.03})$

TABLE 6.11
Number of iterations, condition number, discrete norm errors, and convergence rates for Example 3: *discontinuous linear mortars and matching grids.*

$1/h$	Iter.	Cond.	$\|\|p-p_h\|\|$	$\|\|\mathbf{u}-\mathbf{u}_h\|\|$	$\|\|\|p-p_h\|\|\|$	$\|\|\|\mathbf{u}-\mathbf{u}_h\|\|\|$	$\|\|\|p-\lambda_H\|\|\|$
4	10	3.48E+0	4.33E-1	1.01E-1	1.87E-2	3.27E-3	1.42E-2
8	13	5.30E+0	2.17E-1	5.04E-2	4.47E-3	1.30E-3	3.42E-3
16	15	7.64E+0	1.08E-1	2.52E-2	1.09E-3	4.60E-4	8.38E-4
32	16	1.05E+1	5.41E-2	1.26E-2	2.69E-4	1.60E-4	2.08E-4
64	19	1.40E+1	2.71E-2	6.29E-3	6.69E-5	5.58E-5	5.17E-5
Rate			$\mathcal{O}(h^{1.00})$	$\mathcal{O}(h^{1.00})$	$\mathcal{O}(h^{2.03})$	$\mathcal{O}(h^{1.48})$	$\mathcal{O}(h^{2.02})$

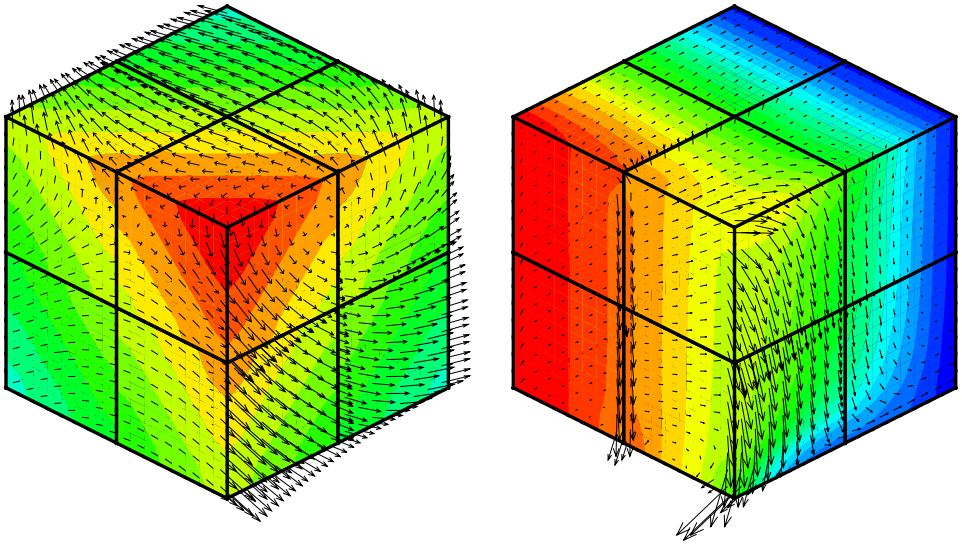

(a) *Solution* (b) *Error*

FIG. 6.3. *Computed pressure (shade) and velocity (arrows) for Example* 3: *continuous quadratic mortars and matching grids.*

Convergence rates are given in Tables 6.10 and 6.11, again confirming the theoretical results. Note that even though this is a problem with a full tensor K, the computed rates exceed the predicted ones (e.g., in Table 6.10, for the discrete pressure error, we expect a rate of 1.25 but observe 2.02). The computed solution and error in pressure and velocity for the case of continuous quadratic mortars on the first level of refinement for matching grids are shown in Figure 6.3.

6.4. Example 4. In the fourth example, we study the behavior of the method as we vary the number of subdomains and the degree of the mortar approximating

TABLE 6.12

Number of iterations, number of flops, and discrete norm errors for Example 4: *continuous quadratic mortars and multiple domains.*

Dom.	Iter.	$\|\|p-p_h\|\|$	$\|\|\mathbf{u}-\mathbf{u}_h\|\|$	$\|\|\|p-p_h\|\|\|$	$\|\|\|\mathbf{u}-\mathbf{u}_h\|\|\|$	$\|\|\|p-\lambda_H\|\|\|$
2×2	16	4.97E-3	4.31E-3	1.61E-5	2.43E-5	1.37E-5
4×4	23	4.97E-3	4.31E-3	1.62E-5	5.20E-5	2.48E-5
8×8	23	4.97E-3	4.31E-3	1.63E-5	9.28E-5	3.83E-5

TABLE 6.13

Number of iterations, number of flops, and discrete norm errors for Example 4: *continuous linear mortars and multiple domains.*

Dom.	Iter.	$\|\|p-p_h\|\|$	$\|\|\mathbf{u}-\mathbf{u}_h\|\|$	$\|\|\|p-p_h\|\|\|$	$\|\|\|\mathbf{u}-\mathbf{u}_h\|\|\|$	$\|\|\|p-\lambda_H\|\|\|$
2×2	23	4.97E-3	4.31E-3	1.61E-5	2.27E-5	1.35E-5
4×4	36	4.97E-3	4.31E-3	1.61E-5	2.78E-5	2.27E-5
8×8	39	4.97E-3	4.31E-3	1.61E-5	3.74E-5	3.41E-5

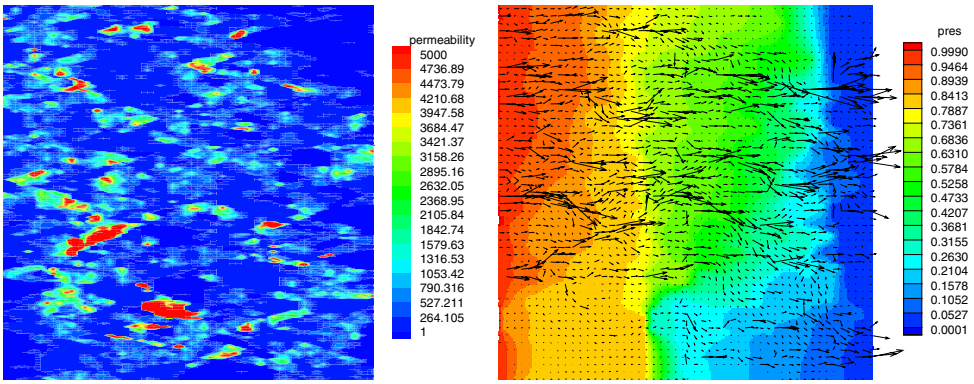

(a) *Permeability* (b) *Solution*

FIG. 6.4. *Permeability field and computed pressure (shade) and velocity (arrows) for Example* 5: *discontinuous quadratic mortars and matching grids.*

functions. The analytic solution and the tensor coefficient are as in Example 1. The fine grid of 256×256 elements was split into three different domain decompositions (coarse grids) of 2×2, 4×4, and 8×8 subdomains. The mortar grids were chosen to be consistent with the optimal choice for velocity superconvergence, i.e., $H=h^{1/2}$ for quadratic mortars and $H=2h$ for linear mortars.

Convergence rates and the number of interface iterations for this test case are given in Tables 6.12 and 6.13. We conclude from the results of this test case that the method scales very well when increasing the number of subdomains. In fact, even though the number of interface iterations increases slightly for more subdomains, the overall cost remains about the same, since the subdomain problems become smaller. In addition, for a given domain decomposition, a comparison between linear and quadratic mortars again confirms the better efficiency of the latter.

6.5. Example 5. In this example, we compare the performance of discontinuous linear and quadratic mortars on a problem with a highly heterogeneous coefficient. The permeability field, shown in Figure 6.4(a), is obtained from the SPE Comparative Solution Project (www.spe.org/csp) and varies more than five orders of magnitude. We simulate flow from left to right. The computed solution on the finest level is

TABLE 6.14

Number of iterations and condition number for Example 5: *discontinuous mortars and matching grids.*

$1/h$	Iter.	Cond.
4	4	8.62E+0
16	17	4.87E+1
64	22	4.51E+1
256	26	3.12E+1

Quadratic mortars

$1/h$	Iter.	Cond.
4	4	4.38E+0
8	11	2.18E+1
16	19	9.35E+1
32	25	1.04E+2
64	25	5.00E+1
128	24	4.42E+1
256	35	3.82E+2

Linear mortars

presented in Figure 6.4(b). In Table 6.14, we report the number of iterations and condition number. We note that on the finest level the discontinuous quadratic mortars are about 30% more efficient than the discontinuous linear mortars. This is similar to what was observed for continuous mortars in the previous smooth examples.

6.6. Adaptive mesh refinement. In the last two examples, we test the performance of the residual-based error estimator. The estimator is used as a local error indicator that drives an adaptive mesh refinement process. The following algorithm describes the adaptive procedure.

GRID REFINEMENT ALGORITHM.

1. Solve the problem on a coarse subdomain and mortar grid.
2. For each subdomain Ω_i:
   (a) Compute
$$\omega_i = \left(\sum_{E \in \mathcal{T}_{h,i}} \omega_E^2 + \sum_{\tau \in \mathcal{T}^{\Gamma_i, H}} \omega_\tau^2 \right)^{1/2};$$
   (b) If $\omega_i > .5 \max_{1 \le j \le n} \omega_j$, refine $\mathcal{T}_{h,i}$.
3. For each interface $\Gamma_{i,j}$, if either Ω_i or Ω_j has been refined m times, refine $\mathcal{T}_{H,i,j}$.
4. Solve the problem on the refined grid. If either the desired error tolerance or the maximum refinement level has been reached, exit; otherwise, go to step 2.

Note that we employ the pressure error estimator based on ω_E and ω_τ, defined in (5.7) and (5.8), since it provides an efficient and reliable estimate of the L^2-pressure error, due to Theorems 5.1 and 5.3 (see also Remark 5.2). Also, according to step 3, the mortar grids are refined if either adjacent subdomain grid is refined sufficiently many times (depending on the mortar polynomial degree m).

For these last two examples, the unit square domain is decomposed into 6×6 subdomains. The coarse grid in each subdomain is 2×2 with a single mortar element on each interface. Both continuous and discontinuous piecewise quadratic mortar spaces on the interfaces were tested.

6.6.1. Example 6. In Example 6, we test a problem with a boundary layer. The true pressure is
$$p(x, y) = 1000\, x\, y\, e^{-10(x^2+y^2)},$$
with $K = I$. The computed pressures after three refinements for the cases of discontinuous quadratic and linear mortars are shown in Figure 6.5. Observe that the

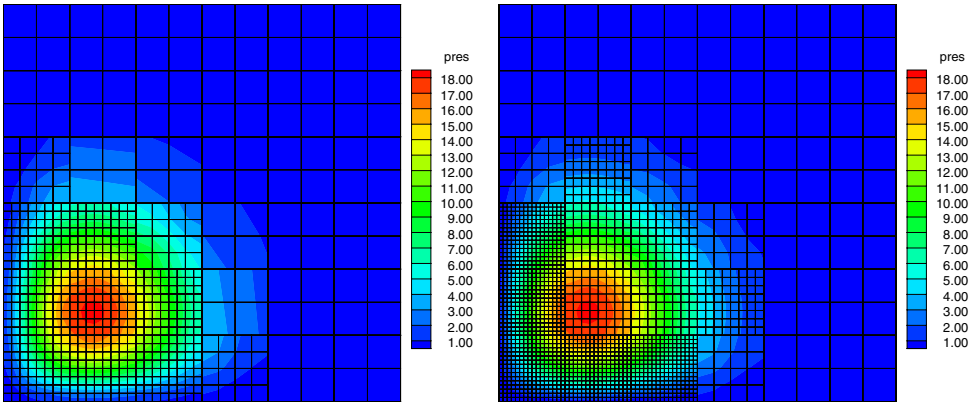

(a) *Discontinuous quadratic mortars* (b) *Discontinuous linear mortars*

FIG. 6.5. *Computed pressure on the fourth grid level for Example* 6.

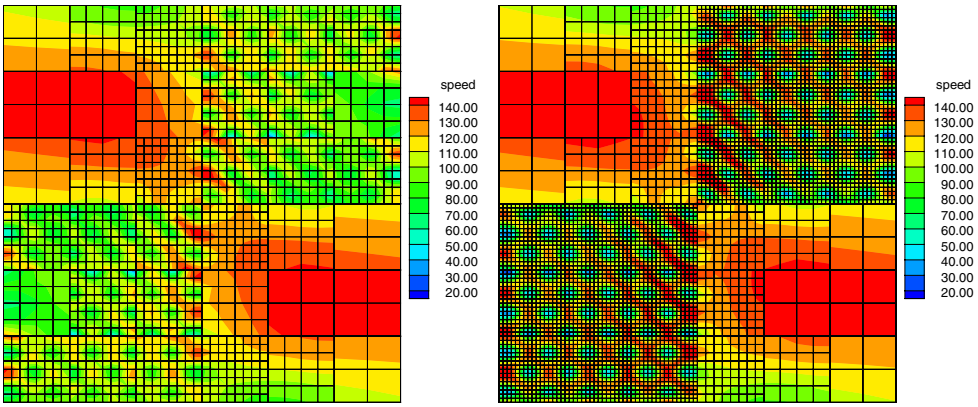

(a) *Continuous quadratic mortars* (b) *Continuous linear mortars*

FIG. 6.6. *Computed magnitude of the velocity on the fifth grid level for Example* 7.

linear mortars produce finer grids that are appropriately refined along the boundary layer, while the quadratic mortars give grids that are coarser and more uniform in that region.

6.6.2. Example 7. In the last example, we test a problem with a highly oscillating tensor:

$$K = \begin{cases} 105 - 100\sin(20\pi x)\sin(20\pi y), & x, y \in [0, 1/2] \text{ or } x, y \in [1/2, 1], \\ 105 - 100\sin(2\pi x)\sin(2\pi y), & \text{otherwise.} \end{cases}$$

The computed magnitude of the velocity after four refinements for the cases of continuous quadratic and linear mortars are shown in Figure 6.6.

Note that the highly oscillating velocity is well resolved by the fine computational grid in the lower-left and the upper-right regions. Some refinement is also observed along the line $x = 1/2$ due to the large jump-flux term ω_τ. As in the previous example, linear mortars produce finer grids, especially in the two regions of high oscillation.

REFERENCES

[1] J. E. Aarnes, *On the use of a mixed multiscale finite element method for greater flexibility and increased speed or improved accuracy in reservoir simulation*, Multiscale Model. Simul., 2 (2004), pp. 421–439.

[2] J. E. Aarnes, S. Krogstad, and K.-A. Lie, *A hierarchical multiscale method for two-phase flow based upon mixed finite elements and nonuniform coarse grids*, Multiscale Model. Simul., 5 (2006), pp. 337–363.

[3] T. Arbogast, *Analysis of a two-scale, locally conservative subgrid upscaling for elliptic problems*, SIAM J. Numer. Anal., 42 (2004), pp. 576–598.

[4] T. Arbogast and K. J. Boyd, *Subgrid upscaling and mixed multiscale finite elements*, SIAM J. Numer. Anal., 44 (2006), pp. 1150–1171.

[5] T. Arbogast, L. C. Cowsar, M. F. Wheeler, and I. Yotov, *Mixed finite element methods on nonmatching multiblock grids*, SIAM J. Numer. Anal., 37 (2000), pp. 1295–1315.

[6] T. Arbogast, C. N. Dawson, P. T. Keenan, M. F. Wheeler, and I. Yotov, *Enhanced cell-centered finite differences for elliptic equations on general geometry*, SIAM J. Sci. Comput., 19 (1998), pp. 404–425.

[7] T. Arbogast, S. E. Minkoff, and P. T. Keenan, *An operator-based approach to upscaling the pressure equation*, in Computational Methods in Water Resources XII, Vol. 1: Computational Methods in Contamination and Remediation of Water Resources, V. N. Burganos, G. Karatzas, A. Payatakes, C. Brebbia, W. Gray, and G. Pinder, eds., Computational Mechanics Publications, Southampton, UK, 1998, pp. 405–412.

[8] T. Arbogast, M. F. Wheeler, and I. Yotov, *Mixed finite elements for elliptic problems with tensor coefficients as cell-centered finite differences*, SIAM J. Numer. Anal., 34 (1997), pp. 828–852.

[9] T. Arbogast and I. Yotov, *A non-mortar mixed finite element method for elliptic problems on non-matching multiblock grids*, Comput. Methods Appl. Mech. Engrg., 149 (1997), pp. 255–265.

[10] D. N. Arnold and F. Brezzi, *Mixed and nonconforming finite element methods: Implementation, postprocessing and error estimates*, RAIRO Modél. Math. Anal. Numér., 19 (1985), pp. 7–32.

[11] C. Bernardi, Y. Maday, and A. T. Patera, *A new nonconforming approach to domain decomposition: The mortar element method*, in Nonlinear Partial Differential Equations and Their Applications, H. Brezis and J. L. Lions, eds., Longman Scientific and Technical, Harlow, UK, 1994.

[12] F. Brezzi, *Interacting with the subgrid world*, in Numerical Analysis 1999, Chapman and Hall/CRC, Boca Raton, FL, 2000, pp. 69–82.

[13] F. Brezzi, J. Douglas, Jr., R. Durán, and M. Fortin, *Mixed finite elements for second order elliptic problems in three variables*, Numer. Math., 51 (1987), pp. 237–250.

[14] F. Brezzi, J. Douglas, Jr., M. Fortin, and L. D. Marini, *Efficient rectangular mixed finite elements in two and three space variables*, RAIRO Modél. Math. Anal. Numér., 21 (1987), pp. 581–604.

[15] F. Brezzi, J. Douglas, Jr., and L. D. Marini, *Two families of mixed elements for second order elliptic problems*, Numer. Math., 88 (1985), pp. 217–235.

[16] F. Brezzi and M. Fortin, *Mixed and Hybrid Finite Element Methods*, Springer-Verlag, New York, 1991.

[17] Z. Chen and J. Douglas, Jr., *Prismatic mixed finite elements for second order elliptic problems*, Calcolo, 26 (1989), pp. 135–148.

[18] Z. Chen and T. Y. Hou, *A mixed multiscale finite element method for elliptic problems with oscillating coefficients*, Math. Comp., 72 (2003), pp. 541–576.

[19] P. G. Ciarlet, *The Finite Element Method for Elliptic Problems*, Stud. Math. Appl. 4, North–Holland, Amsterdam, 1978; reprinted, SIAM, Philadelphia, 2002.

[20] L. C. Cowsar, J. Mandel, and M. F. Wheeler, *Balancing domain decomposition for mixed finite elements*, Math. Comp., 64 (1995), pp. 989–1015.

[21] J. Douglas, Jr., and J. E. Roberts, *Global estimates for mixed methods for second order elliptic equations*, Math. Comp., 44 (1985), pp. 39–52.

[22] R. Durán, *Superconvergence for rectangular mixed finite elements*, Numer. Math., 58 (1990), pp. 287–298.

[23] R. E. Ewing, R. D. Lazarov, T. F. Russell, and P. S. Vassilevski, *Local refinement via domain decomposition techniques for mixed finite element methods with rectangular Raviart-Thomas elements*, in Third International Symposium on Domain Decomposition Methods for Partial Differential Equations, T. F. Chan, R. Glowinski, J. Périaux, and O. B. Widlund, eds., SIAM, Philadelphia, 1990, pp. 98–114.

[24] R. E. Ewing, R. D. Lazarov, and J. Wang, *Superconvergence of the velocity along the Gauss lines in mixed finite element methods*, SIAM J. Numer. Anal., 28 (1991), pp. 1015–1029.
[25] R. E. Ewing and J. Wang, *Analysis of mixed finite element methods on locally refined grids*, Numer. Math., 63 (1992), pp. 183–194.
[26] D. Gilbarg and N. S. Trudinger, *Elliptic Partial Differential Equations of Second Order*, Springer-Verlag, Berlin, 1983.
[27] R. Glowinski and M. F. Wheeler, *Domain decomposition and mixed finite element methods for elliptic problems*, in First International Symposium on Domain Decomposition Methods for Partial Differential Equations, R. Glowinski, G. H. Golub, G. A. Meurant, and J. Périaux, eds., SIAM, Philadelphia, 1988, pp. 144–172.
[28] P. Grisvard, *Elliptic Problems in Nonsmooth Domains*, Pitman, Boston, 1985.
[29] T. Y. Hou and X. H. Wu, *A multiscale finite element method for elliptic problems in composite materials and porous media*, J. Comput. Phys., 134 (1997), pp. 169–189.
[30] T. Y. Hou, X.-H. Wu, and Z. Cai, *Convergence of a multiscale finite element method for elliptic problems with rapidly oscillating coefficients*, Math. Comp., 68 (1999), pp. 913–943.
[31] T. J. R. Hughes, *Multiscale phenomena: Green's functions, the Dirichlet-to-Neumann formulation, subgrid scale models, bubbles and the origins of stabilized methods*, Comput. Methods Appl. Mech. Engrg., 127 (1995), pp. 387–401.
[32] T. J. R. Hughes, G. R. Feijóo, L. Mazzei, and J.-B. Quincy, *The variational multiscale method—a paradigm for computational mechanics*, Comput. Methods Appl. Mech. Engrg., 166 (1998), pp. 3–24.
[33] P. Jenny, S. H. Lee, and H. A. Tchelepi, *Multi-scale finite-volume method for elliptic problems in subsurface flow simulation*, J. Comput. Phys., 187 (2003), pp. 47–67.
[34] J. L. Lions and E. Magenes, *Non-Homogeneous Boundary Value Problems and Applications*, Vol. 1, Springer-Verlag, New York, Heidelberg, 1972.
[35] T. P. Mathew, *Domain Decomposition and Iterative Refinement Methods for Mixed Finite Element Discretizations of Elliptic Problems*, Ph.D. thesis, Tech. report 463, Courant Institute of Mathematical Sciences, New York University, New York, NY, 1989.
[36] M. Nakata, A. Weiser, and M. F. Wheeler, *Some superconvergence results for mixed finite element methods for elliptic problems on rectangular domains*, in The Mathematics of Finite Elements and Applications, V (Uxbridge, 1984), Academic Press, London, 1985, pp. 367–389.
[37] J. C. Nédélec, *Mixed finite elements in* $\mathbf{R}^3$, Numer. Math., 35 (1980), pp. 315–341.
[38] G. Pencheva and I. Yotov, *Balancing domain decomposition for mortar mixed finite element methods on non-matching grids*, Numer. Linear Algebra Appl., 10 (2003), pp. 159–180.
[39] R. A. Raviart and J. M. Thomas, *A mixed finite element method for 2nd order elliptic problems*, in Mathematical Aspects of the Finite Element Method, Lecture Notes in Math. 606, Springer-Verlag, New York, 1977, pp. 292–315.
[40] J. E. Roberts and J.-M. Thomas, *Mixed and hybrid methods*, in Handbook of Numerical Analysis, Vol. II, P. G. Ciarlet and J. Lions, eds., North–Holland, Amsterdam, 1991, pp. 523–639.
[41] L. R. Scott and S. Zhang, *Finite element interpolation of nonsmooth functions satisfying boundary conditions*, Math. Comp., 54 (1990), pp. 483–493.
[42] J. M. Thomas, *Sur l'analyse numerique des methodes d'elements finis hybrides et mixtes*, Ph.D. thesis, Sciences Mathematiques, Université Pierre et Marie Curie, Paris, France, 1977.
[43] A. Weiser and M. F. Wheeler, *On convergence of block-centered finite differences for elliptic problems*, SIAM J. Numer. Anal., 25 (1988), pp. 351–375.
[44] M. F. Wheeler and I. Yotov, *A posteriori error estimates for the mortar mixed finite element method*, SIAM J. Numer. Anal., 43 (2005), pp. 1021–1042.
[45] B. I. Wohlmuth and R. H. W. Hoppe, *A comparison of a posteriori error estimators for mixed finite element discretizations by Raviart-Thomas elements*, Math. Comp., 68 (1999), pp. 1347–1378.
[46] I. Yotov, *Mixed Finite Element Methods for Flow in Porous Media*, Ph.D. thesis, Rice University, Houston, TX, 1996. Also TR96-09, Department of Computational and Applied Mathematics, Rice University and TICAM report 96-23, University of Texas at Austin.